5 UAV LiDAR surveys and machine learning improves snow depth and water equivalent estimates in boreal landscapes

Maiju Ylönen¹, Hannu Marttila¹, Joschka Geissler², Anton Kuzmin³, Pasi Korpelainen³, Timo Kumpula³, Pertti Ala-Aho¹

- ¹ Water, Energy and Environmental Engineering Research Unit, University of Oulu, Oulu, 90014, Finland
- ² Faculty of Environment and Natural Sciences, University of Freiburg, 79098 Freiburg, Germany
 - ³ Department of Geographical and Historical Studies, University of Eastern Finland, 80101, Joensuu, Finland

Correspondence to: Maiju Ylönen (maiju.ylonen@oulu.fi)

Abstract

10

15

20

25

30

35

40

45

Climate change is rapidly altering snow conditions worldwide and northern regions are experiencing particularly significant impacts. As these regions are experiencing warming faster than the global average, understanding snow distribution and its properties at both global and local scales is critical for effective water resource management and environmental protection. While satellite data and point measurements provide valuable information for snow research and models, they are often insufficient for capturing local-scale variability. To address this gap, we integrated UAV LiDAR with daily reference measurements, snow course measurements and a machine learning (ML) approach. By using ML clustering, we generated high-resolution (1 m) snow depth and snow water equivalent (SWE) maps for two study areas in northern Finland. Data was collected through four different field campaigns during the 2023-2024 winter season. The results indicate that snow distribution in the study areas can be classified into three categories based on land cover: forested areas, transition zones with bushes, and open areas (namely peatlands), each showing different snow accumulation and ablation dynamics. Cluster-based modelled SWE values for the snow courses gave good overall accuracy, with RMSE values of 31-36 mm. Compared to snow course measurements, the cluster-based model approach enhances the spatial and temporal coverage of continuous SWE estimates, offering valuable insights into local snow patterns at the different sites. Our study highlights the influence of forests and forest gaps on snow accumulation and melt processes, emphasizing their role in shaping snow distribution patterns across different landscape types in the arctic boreal zone. The results improve boreal snow monitoring and water resource management, offer new tools and high-resolution spatiotemporal data for local stakeholders working with hydrological forecasting and climate adaptation and support satellite-based observations.

Keywords: remote sensing, drones, snow, arctic, mapping, spatial

1 Introduction

Snow is an important part of the hydrological cycle and is highly relevant for societies and ecosystems, especially in high latitudes and mountainous regions. Snow cover, timing and distribution directly influences climate energy budget through snow albedo (Callaghan et al., 2011; Li et al., 2018), ecosystems and habitats, including species and vegetation distribution (Thiebault & Young, 2020), biogeochemical processes in soils and seasonal ground frost (Ala-Aho et al., 2021; Croghan et al., 2023; Jan & Painter, 2020). Additionally, snow resources have a major impact on catchment, river and groundwater budgets, and seasonal distribution (Meriö et al., 2019). Snow-covered areas are decreasing as global temperatures rise, leading to a consistent decline in snow water equivalent (SWE) (Colombo et al., 2022; Faquseh & Grossi, 2024; Kunkel et al., 2016; Räisänen, 2023; Y. Zhang & Ma, 2018). A recent study by Gottlieb & Mankin (2024) shows how March SWE has decreased in half of the Northern Hemisphere river basins over the past 40 years with the highest decreases in the southwestern USA and western, central and northern Europe. The timing and amount of snowmelt, along with SWE in the melting period, are crucial for local water balance and flood

monitoring and regulation (Bavay et al., 2013; Callaghan et al., 2011; Wang et al., 2016). Changes in snow conditions and rising temperatures are causing earlier flood peaks in snowmelt-dominated catchments with a decline in streamflow later in the year (Berghuijs & Hale, 2025; Engelhardt et al., 2014; Matti et al., 2017). Snowmelt significantly influences near-surface hydrological effects (Muhic et al., 2023) and soil moisture in these regions (Okkonen et al., 2017).

50

55

60

65

70

75

80

85

90

Snow models are an important part of water resource planning and prediction. These models provide estimations of snow related hydrological parameters for areas and times where ground observations are not available and can be used for creating various scenarios. However, for the accurate prediction of snow-water resources, snow models require high-resolution data as inputs, testing and validation. Satellite based remote sensing is still a rather coarse tool and has limited accuracy with canopy cover (Muhuri et al., 2021; Rittger et al., 2020). For example, currently, the accuracy and spatiotemporal availability of SWE from microwave satellite missions is not sufficient for local scale water resource management planning (Tsang et al., 2022a). Gaffey & Bhardwaj (2020)concludes that as only a few satellite sensors provide resolution required to capture local variability with multispectral or infrared data, together with limited revisiting times, the usage of satellite products in snow research is still limited. Thus, ground-based manual measurements, which are then fed to operational models, are still conducted. The national snow course measurement network – a manual snow depth and density measurement protocol - provides important data for models and serves as a long-term historical dataset; however, this is time-consuming, the accuracy varies (Beaudoin-Galaise & Jutras, 2022; Kuusisto, 1984; Mustonen, 1965), and temporal resolution is weeks to month. Thus, it is not ideal for capturing snow dynamics of individual events or important hydrological variables such as peak snow depth or melt-out dates (Malek et al., 2020).

To bridge the knowledge and technical gap between remotely sensed and ground observations, uncrewed aerial vehicles (UAV) have been proven to be efficient in snow depth and SWE estimations, providing decent cost efficiency and accuracy (Adams et al., 2018; Niedzielski et al., 2018; Rauhala et al., 2023). Like satellite platforms, UAV systems can carry both optical and radar-based sensors and provide high resolution spatial information. Photogrammetry, including multispectraland stereo-imagery, can result in centimeter-scale accuracy in snow depth mapping over a catchment scale and is relatively low cost compared to radars like ground-penetrating radar (GPR) and light detection and ranging (LiDAR) (Maier et al., 2022; Nolan et al., 2015; Rauhala et al., 2023). Combining snow depth data from LiDAR and spectrometer sensors has also been used to model snow density on a weekly basis at the Airborne Snow Observatory (ASO) (Painter et al., 2016) Yet, photogrammetry-based products, like structure-from-motion (SfM), require suited light conditions and heterogeneous snow surfaces and are limited in penetrating dense vegetation covers. Thus, the decision between cost-effectiveness and accuracy is dependent on the site characteristics (Rauhala et al., 2023; Rogers et al., 2020). Recently, LiDAR sensors have become more affordable, compact and lightweight. Technical advancements, such as improved inertial measurement units (IMUs) and global navigation satellite systems (GNSS), have enhanced their accuracy and performance, making LiDAR more cost-effective and competitive compared to UAV photogrammetry (Bhardwaj et al., 2016; Rogers et al., 2020). The UAV LiDAR technology potentially offers high accuracy over large spatial areas and allows catchment-scale mapping even under canopy cover, unaffected by overcast conditions or shadows (Dharmadasa et al., 2022; Harder et al., 2020; Jacobs et al., 2021; Mazzotti et al., 2019). LiDAR based snow depth data, when combined with models or density assumptions, can also be used to estimate the spatial distribution of SWE on a landscape scale, with decent cost-effectiveness (Broxton et al., 2019; Geissler et al., 2023).

Snow conditions are mostly controlled by temperature and precipitation (Mudryk et al., 2020; Mudryk et al., 2017), and changes in global and local climate trends impact snow cover differently across regions. However, local snow accumulation is dependent on on-site characteristics, such as topography, vegetation, weather and wind patterns (Currier & Lundquist, 2018; Mazzotti et al., 2019, 2023). Forest structure significantly affects snow accumulation (Mazzotti et al., 2023), and SWE values for forested areas appear significantly higher than in tundra and shrub tundra zones (Busseau et al., 2017; Dharmadasa et al., 2023). The effect of forest canopy on snow melt also depends on the

climate, because in cold regions, the snow lasts longer in forests, whereas in warm climates, it stays longer in forest openings (Lundquist et al., 2013). Additionally, snowpack characteristics are spatially different in forest gaps (Bouchard et al., 2022) and edges (Currier et al., 2022; Mazzotti et al., 2019). Vegetation changes, such as the northward retreat of the tree line, the densification of existing vegetation and the migration of new species towards the poles, will also affect snow dynamics; these effects are not yet fully known (Aakala et al., 2014; Franke et al., 2017; Grace et al., 2002; Ropars & Boudreau, 2012). To enhance our understanding of snow processes in sub-arctic and boreal regions, we need improved tools and approaches, especially with localized high resolution spatial data.

105

110

115

120

125

130

135

Even though annual changes in snow cover are dominated by weather conditions, different patterns of snow distribution and melting can be detected (Currier et al., 2022; Geissler et al., 2023; Matiu et al., 2021). These snow distribution patterns are site-specific and are dictated by local site characteristics, and, importantly, they can be extended to different years (Pflug & Lundquist, 2020; Sturm & Wagner, 2010). Yet, the approach of Pflug & Lundquist (2020) would require several years of snow depth maps from the regions, which is not always feasible. Revuelto et al. (2020) successfully modeled daily snow depth maps using in-situ measurements and time-lapse photographs, and field data collected from two winters was estimated to be enough for the random forest model to estimate snow depth for other years. Repetitive UAV surveys over winter seasons can provide spatial information on snow cover, helping the identification of factors affecting snow distribution. Different machine learning approaches have shown promising results in snow depth and SWE mapping for different regions (J. Zhang et al., 2021), as they can reduce biases and enhance overall accuracy (King et al., 2020; Vafakhah et al., 2022). ClustSnow, a ML framework based on kMeans and random forest clustering, first presented in Geissler et al. 2023, allows the determination of snow patterns (referred to as clusters) from repetitive spatial snow depth maps only. These clusters can not only characterize areas with similar seasonal snow dynamics, but also serve as a temporally persistent extrapolation basis (Geissler et al. 2024) of local field observations or sensor measurements, enabling the creation of daily spatial snow depth and SWE maps of entire winter seasons with accuracies in the same magnitudes as the underlying data or modern snow models. However, ClustSnow requires a network of sensors that is not feasible for many sites and was yet only tested on very small sites (0.22 km²) within central Europe. So far, the ClustSnow framework has, however, not been tested within sub-arctic and boreal regions. (Meloche et al., 2022; Revuelto et al., 2020)(Geissler et al., 2023)

Our study produces daily spatial snow depth and SWE estimates in different sites based on a combination of LiDAR-based snow depth maps, snow course measurements, and continuous snow depth measurements. The field data was collected during winter 2023-24 from two different sites in Finnish Lapland, each with long-term monitoring infrastructure and existing snow course measurements, representing different vegetational and topographical conditions typical for boreal and sub-arctic landscapes. The study applies ClustSnow workflow (Geissler et al., 2023, 2024), a ML model based on spatially similar snow depth zones, to novel data and regions with different climatic and environmental conditions. To our knowledge, this method has not yet been used in boreal and sub-arctic areas but has proven to be a promising approach in the Alpine conditions. In comparison to the original study by Geissler et al. (2023) this study applies the model with fewer ultrasonic sensors and LiDAR surveys, with new climate and larger study areas. We also examine the ability of the UAV LiDAR to map snow depth in forested boreal and subarctic areas in northern Finland and discuss how machine learning-derived snow depth clusters and properties could be used to improve SWE estimates in our study areas with considerably better spatial and temporal resolution compared to traditional operational snow course measurements.

2 Data and methods

2.1 Study areas

Two study areas were chosen to present different environmental conditions for Finnish Lapland and sub-arctic and boreal zones, namely Pallas (Fig. 1a) and Sodankylä (Fig. 1b). Both sites have on-going snow course measurements operated by the Finnish Environment Institute (SYKE), at least one ultrasonic snow depth sensor together with weather station operated by the Finnish Meteorological institute (FMI). Data collected by SYKE and FMI is publicly available (Sect. 2.2.4).

145

150

Pallas (67° 59' N, 24° 14' E) is the northernmost of the study sites and is located the highest from sea level. The land cover is mostly coniferous forests (63%), with mires and mixed forests (Table 1). It has higher average snow depths compared to Sodankylä. Sodankylä is located in the middle part of Lapland (67° 21' N, 26° 37' E), the land cover is mainly mire (63%), and the elevation range is low (Table 1). The Sodankylä site is part of the FMI research station, which has daily weather observations starting from 1908 (The Finnish meteorological institute, 2025).

Table 1. Meteorological and landscape characteristics for Pallas and Sodankylä.

	Pallas	Sodankylä	Data source
Elevation range (m)	267-350	178-183	NLS
Mean annual air temperature (°C) 2008-2024	0.5	0.9	FMI
Mean annual total precipitation (mm) 2008-2024	644	553	FMI
Average snow depth Nov-May (cm) 2008-2024	65	48	FMI
Average winter wind direction Nov-Apr (°)	199	182	FMI
Lidar extent (km²)	0.8	1.1	
Land cover (%): deciduous	0.1	0.1	SYKE Corine land cover 2018
coniferous	62.7	27.0	
Mixed	14.9	3.7	
Mire	17.2	62.7	
canopy closure <30 %	3.5	4.1	

Data sources: FMI (2025), SYKE (2018), National Land Survey of Finland (NLS) (2020).

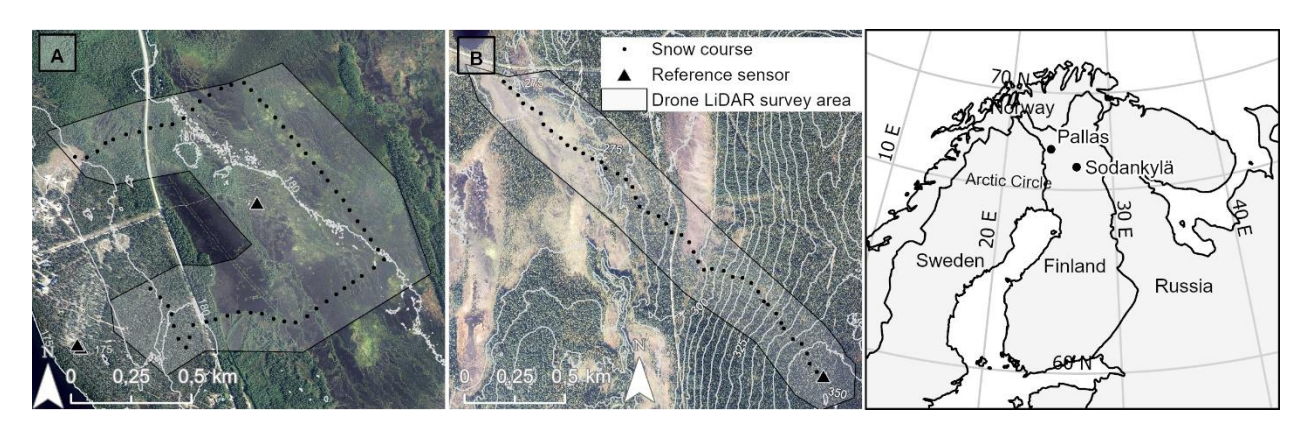


Figure 1. The location and maps of study sites (a) Sodankylä and (b) Pallas. The gray area represent UAV-flight areas, and the black points mark the manual snow sampling locations of the snow courses. Orthophoto were obtained from the National Land Survey of Finland.

2.2 Field measurements

160

165

170

175

180

In our field campaigns, one snow-off and four snow-on LiDAR surveys were conducted in both sites during the winter of 2023-2024. Snow-on campaigns were carried out at the beginning of January, the end of March, the end of April, and the beginning of May, whereas the snow-off campaigns were conducted on May 30th for Sodankylä and June 7th for Pallas, just after snow melting and before the new vegetation growth season. The aim was to capture the snowpack in its different winter stages (i) new snowpack, ii) maximum snowpack, and iii) late, melting snowpack) to distinguish areas in each site with similar snow patterns and variability (Fig. 2). During winter 2023-2024, the snow depths were above the average in Pallas and Sodankylä. At both sites, snow ablation started in March 2024, interrupted by some major snowfall events in April 2024 (Fig. S4, supplementary materials).

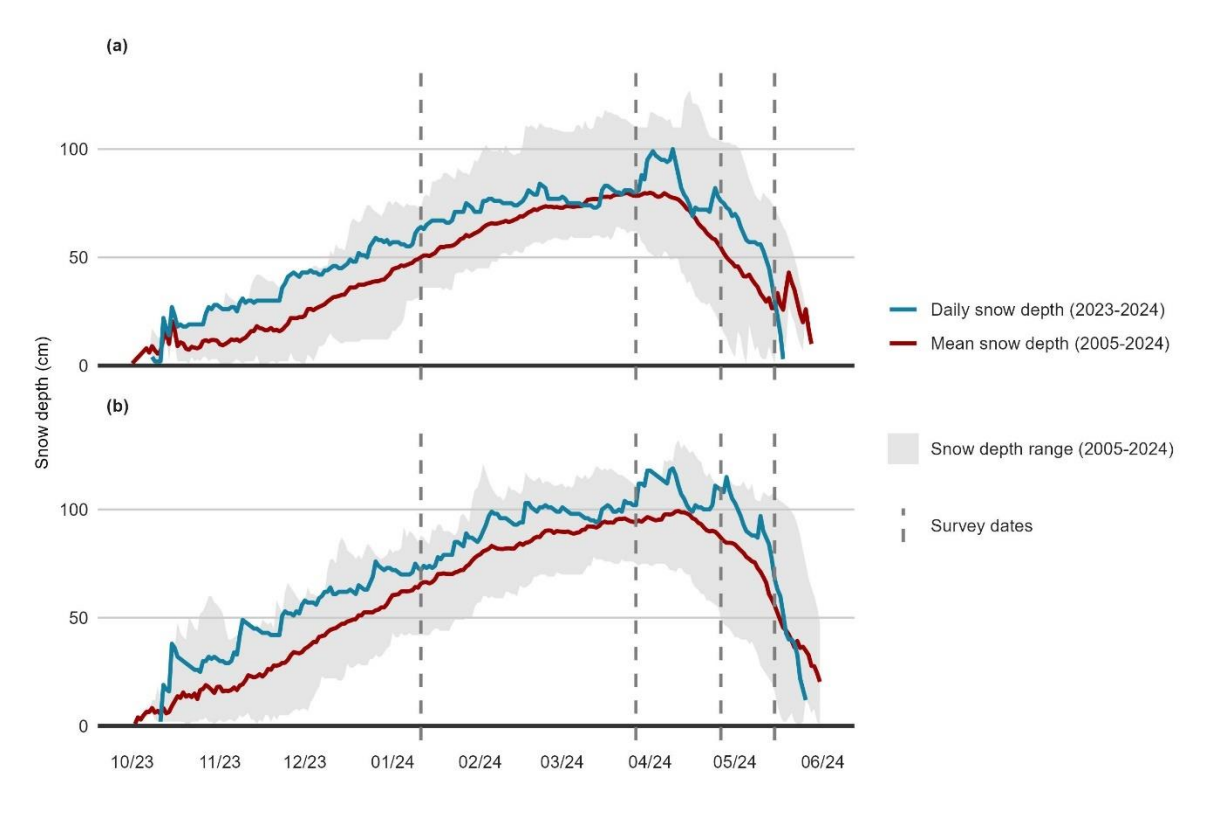


Figure 2. Snow depths from each site's FMI stations. Sodankylä (a), and Pallas (b). Dark dashed lines represent the UAV campaign dates from the winter of 2023-2024. The red line represents the long-term average snow depth (2005-2024) and blue lines the daily snow depths of this study's winter season 2023-2024.

2.2.1 UAV LiDAR surveys

UAV LiDAR mapping was performed at Sodankylä and Pallas using YellowScan Mapper+ (YellowScan, France), equipped with an Applanix APX-15 inertial measurement unit and mounted on a DJI Matrice 300 RTK (DJI, Shenzhen, China). The scanner operated with a 70.4° scanning angle and a 240 kHz pulse repetition frequency, with both sites scanned at a cruising speed of 7 m/s, an altitude of 80 m above ground level, and a 70% overlap between flight lines (Table S1. appendices). Trajectory correction was carried out in Applanix POSPac software using continuously operating reference station (CORS) observations from the National Land Survey of Finland CORS network as the reference data. For more details on the LiDAR system and flight parameters, see Supplementary materials (Table S1, appendices).

We compared the accuracy of the digital terrain models (DTMs) between different data processing methods, using five GCPs (ground control points) as a reference. In Yellowscan CloudStation, we tested two gridding strategies for DTM generation — MinZ, which uses the minimum elevation value within each grid cell, and MeanZ, which averages the elevation of all ground points for each cell. We also compared the accuracy of the DTMs between different data processing methods, using 5 GCP (ground control point) as a reference. The 5 GCP plates were distributed across the study areas during each campaign and geolocated with RTK GNSS devices, Emlid RS2+ (Hungary) or Trimble GNSS system R12i (USA), which report 7-8mm horizontal and 14-15mm vertical RTK accuracies. Best results were obtained when processing the point clouds with the MinZ method, which was therefore used for the determination of DTMs from the point clouds.

2.2.3 Manual snow measurements

185

190

195

200

205

Manual snow depth and density measurements were conducted within six hours, after the completion of the UAV campaigns. Snow course measurements were carried out following the SYKE snow survey protocol (Kuusisto, 1984; Mustonen, 1965). (Kuusisto, 1984; Mustonen, 1965)Snow depth was measured every 50 m and density every 200 m along the snow course transect in Pallas (Fig. 1a). In Sodankylä, where the snow course is longer (4 km), SWE was measured at eight different sites along the snow course. These measurement locataions were selected to represent different terrain types present in the study site (Fig. 1b). Snow measurement points were geolocated using RTK GNSS Emlid RS2+ (Hungary) and Trimble GNSS system R12i (USA). In Pallas, snow depth was measured using fixed poles installed in the field, whereas in Sodankylä, measurements were taken manually with a wooden snow probe at predefined GPS-marked locations. Obtained data was used as validation data for modelled maps. **2.2.4 Automatic daily snow depth measurements**

Sodankylä is equipped with three ultrasonic sensors (Campbell Scientific SR50) providing daily snow depth recordings (Fig. 1b). The sensors are operated by FMI and the data is open access (https://litdb.fmi.fi/index.php). Sensors are in open peatland (N67°22.024', E26°39.070'), pine forest opening (N67°21.706', E26°38.031') and inside sparse pine forest (N67°21.699', E26°38.051'). Pallas has one ultrasonic sensor (Campbell Scientific SR50) providing daily snow depth data. This sensor is located in Kenttärova (Fig. 1a) and is also operated by FMI (https://en.ilmatieteenlaitos.fi/download-observations). The sensor is located in the spruce forest in the upper part of the study area (N67°59.237', E24°14.579').

2.2.5 Associating manual snow course measurements with automatic snow depth sensors

Manual snow depth measurements from snow courses were linearly interpolated to estimate snow depths between measurement dates. To improve the accuracy of these estimates, the interpolated values were adjusted using daily snow depth changes recorded by the in-situ snow depth sensors (Fig. 1a, 1b). At each snow course measurement point, the interpolated snow depth was corrected by adding the daily change observed at the representative snow depth sensor. Unlike Pallas, where one reference sensor is available, Sodankylä has multiple ultrasonic snow depth sensors distributed across different environments, allowing more representative corrections. Each snow course measurement point is assigned to one of these environmental categories, ensuring that the most appropriate sensor was used for correction. If the corrected snow depth estimate resulted in a negative value, it was set to zero.

2.3 Data analysis

2.3.1 LiDAR data processing

LiDAR data from each campaign was pre-processed using CloudStation software. As part of this process, we performed strip alignment of the flight lines to generate an accurately georeferenced point cloud. To classify points belonging to the ground, we applied the following parameters: steepness (which reflects terrain variation) was set to 0.2, the minimum object height (the vertical threshold above which an object is not considered part of the ground) was

set to 0.03 m, and point cloud thickness was set to 0.15 m. Multiple combinations of parameters—such as minimum object height and slope tolerance — were tested and visually evaluated against field observations and GCPs. The final configuration effectively minimized misclassification and produced the most accurate and realistic DTMs for our boreal study area. The same parameter set was applied consistently across all campaigns, including both bare-ground and snow-covered conditions. Although snow accumulation can smooth terrain features and influence classification (e.g., reducing local slope), the selected settings yielded stable and reliable results across all conditions.

Following classification, we generated DTMs with a 10 cm spatial resolution. MinZ method based DTM showed better correspondence with the GCP plates (Sect. 2.2.1) and was used in the following analysis. The DTMs generated using this method for the May campaign in Sodankylä showed lower accuracy compared to those produced by other methods. Nevertheless, as the DTMs from the other campaigns and sites were the most accurate when processed with CloudStation, we chose to apply the same method consistently across all sites and campaigns, accepting the reduced accuracy for May. In addition, for each campaign, the point cloud data shows increments along the trajectory line borders of approximately 1-5 cm. The uplifts are presumably due to poorer georeferencing of points at the trajectory edges and presumably overlapping points from the two trajectories can cause abnormal surfaces in DTMs. We tried to clean up the data from overlapping points, but the overall accuracy of the DTM was degraded, so we chose to accept the inaccuracies in the UAV flight trajectory edge regions.

Further DTM processing was conducted using ArcGis Pro 3.2.0. The snow depth rasters were generated by calculating the difference between the snow-on and the snow-off DTMs and resampled to 1m resolution. Snow depth values falling outside a reasonable range (< -0.5 m; > 2 m) were set to zero to remove extreme outliers, while minor negative values close to zero were corrected to zero (-0.5 m - 0 m). Missing values were filled by calculating the median value from surrounding cells, using the median of the 5x5 neighboring cells. The data was clipped to the area of interest (AOI), focusing the analysis on the buffer zone of 150 m around the snow courses. The 4 DTMs were then stacked together to be used as an input for the model (Chapter 2.3.2).

The error metrics were calculated using the 5 GCPs distributed in the study areas to compare their accuracy to the derived DTMs following the suggestion of Rauhala et al. (2023). To estimate the uncertainty of generated DTMs, the difference between UAV DTMs and RTK measured GCP elevation (Δz) was calculated following Equation 1:

$$\Delta z_t = DSM s_t - z_{GCP} t, \tag{Eq 1}$$

230

235

240

245

where t is the date of survey, DTM_S is the snow surface elevation from the UAV survey, and z_{GCP} is the GCP elevation measured with RTK.

When the snow depth rasters are derived from two DTMs, their precision was estimated following Equation 2:

$$\boldsymbol{u} = \sqrt{\sigma(\Delta z_t)^2 + \sigma(\Delta z_G)^2}, \tag{Eq 2}$$

where $\sigma(\Delta z_t)$ is the standard deviation for the difference between UAV DTM and RTK measured GCP elevation Δz for every winter campaign and $\sigma(\Delta z_G)$ is the standard deviation for the difference between UAV DTM and RTK measured GCP elevation Δz for the bare-ground campaign.

To estimate the trueness of the calculated snow depth rasters, error propagation for the mean error of snow-on and bare-ground DTMs was calculated. It is calculated by finding the average of the differences between the UAV DTMs and the GCP elevations, following Equation 3:

$$265 m = \mu(\Delta z_t) - \mu(\Delta z_G), (Eq 3)$$

where $\mu(\Delta z_t)$ is the mean error for the difference between each snow-on campaign DTMs and GCPs, and $\mu(\Delta z_G)$ is the mean error for the difference between bare-ground campaign DTMs and GCPs.

2.3.2 Application of ClustSnow to LiDAR data sets

270

275

280

290

295

300

305

We applied the ClustSnow workflow first presented in Geissler et al. 2023 to our dataset. All analyses were performed using R Statistical Software (v.4.3.0, R Core Team, 2023). To obtain clusters, ClustSnow applies the k-means (Hartigan & Wong, 1979) and random forest (Breiman, 2001) algorithms to a stack of snow depth (SD) rasters. Consequently, obtained clusters only rely on multitemporal snow observations and do not contain information on the canopy or topography. As a first step, the k-Means algorithm groups a small subsample of cells based on their similarity in observed snow depths to a user-defined number of clusters. Secondly, these sub-sampled and clustered points are used to train a random forest model that, as a last step, is used to predict the probabilities (w) of all grid cells (ij) to belong to the individual clusters (c). Hereafter, we refer to the ClustSnow output as cluster probabilities (w_{ij,c}) and the map containing the cluster numbers for each cell with the highest predicted probability is referred to as cluster map. Cluster numbers are ordered based on the mean snow depth of the underlying SD raster stack to allow an easier interpretation and comparability. Therefore, the cluster number one is assigned to the cluster with the highest mean snow depth and increases with mean snow depth until the user-defined number of clusters is reached.

2.3.3 Creating daily SD and SWE maps

Cluster probabilities at the snow course measurement locations (ij=s) ($w_{s,c}$), which are assigned by normalizing, so that they sum to one in each cluster according to Equation 4:

285
$$\widehat{w_{s,c}} = \frac{w_{s,c}}{\sum_{s} (w_{s,c})}$$
 (Eq. 4)

The synthetic daily snow depths for each cluster $SD_c(t)$ are calculated by multiplying the normalized probabilities by the snow depth values of the corresponding snow course measurements and summing them for each cluster according to Equation 5:

$$SD_c(t) = \widehat{w_{s,c}} \cdot SD_s(t)$$
 (Eq. 5)

The synthetic snow depth maps $SD_{ij}(t)$ are generated by combining synthetic daily snow depth data $(SD_c(t))$ with cluster probabilities $w_{ij,c}$ and multiplying it with the time series data of that cluster $(SD_c(t))$ according to Equation 6:

$$SD_{ij}(t) = \frac{\sum}{c} (w_{ij,c} \cdot SD_c(t))$$
 (Eq. 6)

The synthetic daily snow depth data for clusters was converted into SWE using semi-empiric Δ snow model (Winkler et al., 2021). The model consists of four modules, namely new snow and overburden, dry compaction, drenching or scaling modules, and each module is activated depending on the change of snow depth between time steps. The model has 7 parameters to be calibrated, where Fontrodona-Bach et al. (2023) suggested that two of them are significantly related to the site-specific climate variables. These two key parameters are maximum density of a snow layer (ρ max) and new snow density (ρ 0). Only Sodankylä has snow measurements allowing the determination of ρ 0. In other sites the model was run with the values of ρ 0 and ρ max provided by Fontrodona-Bach et al. (2023). The rest of the 7 parameters were kept as default on Winkler et al. (2021).

The daily SWE maps $SWE_{ij}(t)$ are calculated using the synthetic snow depth data $SD_c(t)$ as an input for the model and then using the same protocol as for HS maps to upscale the daily SWE estimates for the entire study area using Equation 7:

310
$$SWE_{ij}(t) = \sum_{c} (W_{ij,c} \times SWE_{c}(t))$$
 (Eq. 7)

2.3.4 Model calibration and sensitivity

ClustSnow requires a set of parameters to be defined by the user. Most of these parameters showed no sensitivity in the calibration performed in Geissler et al. (2024). The only and most sensitive parameter of ClustSnow is the number of the clusters (*n_class*) parameter. Different indices were tested to guide this decision using the NbClust R package (v3.0.1; Charrad et al., 2014). For Sodankylä and Pallas these indices suggested an optimal number between one and eight. Besides these indices, we performed a full sensitivity analysis of the ClustSnow workflow following Geissler et al. 2024. Therefore, all model parameters are varied within reasonable ranges and the model was run 1000 times with randomly chosen parameter combinations. The snow products of all model runs are evaluated against manual measurements to obtain mean and variance of different goodness-of-fit metrics (RMSE, MAE, R). The results of the sensitivity analysis performed are presented in the supplementary material (Fig. S1, see appendices).

Based on these results, and the low sensitivities of all parameters, parameter values suggested by Geissler et al. 2023 were used, with the exception for the number of cluster (n_class). For comparability and because of the relatively low topographical variation in our sites, we selected n_class to be three in this study for both sites. This number is lower compared to the four clusters obtained in Geissler et al. 2023 and Geissler et al. 2024, but allows an easier comparison with topographic or vegetation. Yet, to allow a better discussion of the effect of this key parameter on the results, we rerun our analysis with n_class set to the optimum of six, obtained in the sensitivity analysis performed here for comparisons (See Section 3.3.2).

3 Results

315

320

325

3.1 The accuracy of UAV based LiDAR for mapping snow depth in boreal and sub-arctic zones

At all study sites, the snow depth measured from snow courses increased until March, after which it starts to decrease due to spring melting (Table 2). Snow depth variation increased during the melting season, but in the April and May campaigns, the variability stabilized as snow had already melted in most areas. The uncertainty of the derived DTMs were studied by comparing GCP points to the UAV DTMs (Sect. 2.2.1). The difference between UAV LiDAR snow depth maps and RTK measured GCP (Eq. 1) resulted in varying accuracies between sites and campaigns and their RMSEs can be seen in Table 3. Weather conditions as well as the accuracy of RTK signals might cause differences not directly related to the UAV LiDAR.

Table 2. Mean snow depth and SWE values and their standard deviations from manual snow course measurements in different campaigns and sites in winter 2023-2024.

Site	Campaign	Mean snow depth (cm)	Standard deviation	n	Mean SWE (mm)	Standard deviation	n
Pallas	January	73.8	4.2	45	125.9	26.9	12
Pallas	Macrh	98.2	6.3	45	234.5	22.2	11
Pallas	April	95.2	11.6	45	239.7	31.6	12
Pallas	May	46.1	12.3	38	148.9	38.1	11
Sodankylä	January	54.0	5.8	81	90.6	11.8	10
Sodankylä	March	62.1	9.4	81	141.5	25.8	10
Sodankylä	April	46.5	19.3	68	137.9	53.7	6
Sodankylä	May	22.8	6.4	20	94.2	28.7	4

Table 3. The RMSE of the differences between GCP plates and DTMs and the precision and trueness of snow depth maps derived from DTMs in different campaigns and sites (Eq.1; Eq.2; Eq.3).

Metrics	Campaign	Sodankylä (cm)	Pallas (cm)
	January	3.1	6.8
	March	6.5	1.2
RMSE (Eq. 1)	April	5.3	3.8
KWISE (Eq. 1)	May	22.8	7.1
	June	2.4	5.1
	All	11.2	5.3
	January	6.6	8.8
	March	4.5	4.7
Precision (Eq. 2)	April	3.9	6.1
	May	20.8	6.3
	Mean	8.8	6.5
	January	2.7	3.3
	March	5.1	3.2
Trueness (Eq. 3)	April	0.9	3.3
	May	13.2	6.7
	Mean	5.3	4.1

Table 3 also summarizes the precision of snow depth maps from standard deviations for each site calculated by Equation 2. The precision of the snow depth maps in Sodankylä was stable during the winter campaigns, performing best in April (4.5 cm), but had an uncertainty of 20.8 cm in May. In Pallas the precision ranged from 4.7 cm in March to 8.8 cm in January. The error propagation for mean error, meaning the trueness of snow depth maps calculated by Equation 3 are also concluded in Table 3. In Sodankylä, the trueness was the best in April (0.9 cm), decreasing in May up to 13.2 cm, mostly caused by the computation of DTM with flooding of the mire areas. Pallas also had the highest trueness in the beginning of winter with relatively stable accuracies through the winter, ranging from 3.2 cm-3.3 cm in January-April and decreasing in May to 6.7 cm. During the main melting season, localised open water and flooding areas especially in open peatland, cause laser beams to reflect differently in comparison to snow or ground surfaces, which can lead to uncertainties especially when using the minimal elevation derived products. This can therefore affect the quality of May DTMs making them poorer in comparison to other months.

3.2 Cluster characteristics show similarities between sites

The characteristics of clusters derived using ClustSnow and their associated snow conditions at each site were analyzed by grouping snow course measurements and environmental data according to their respective cluster classifications.

3.2.1 Cluster characteristics at Sodankylä

345

350

355

Cluster 1 covers 21% of the total Sodankylä area, typically located in forests or pine mires (Fig. 3). It has an average canopy height of 4.6 m and is located typically less than a meter away from forests (Table 4). This cluster has the highest average modelled snow depth and SWE through the winter. According to the ClustSnow-derived snow products, peak snow depth occurs at 14.3.2024 at 75 cm and peak SWE at 23.4.2024 at 164 mm (Table 4). The ablation started after the peak but snow depth increased again at the end of April due to heavy snowfall events, decreasing rapidly afterwards. From snow course measurements, the points classified to this cluster show their snow depth peak on 26.3.2024 with an average of 72.5 cm snow depth (Fig. S2, supplementary material). None of the 7 SWE measurement points of the snow course were classified to this cluster (Fig. 3).

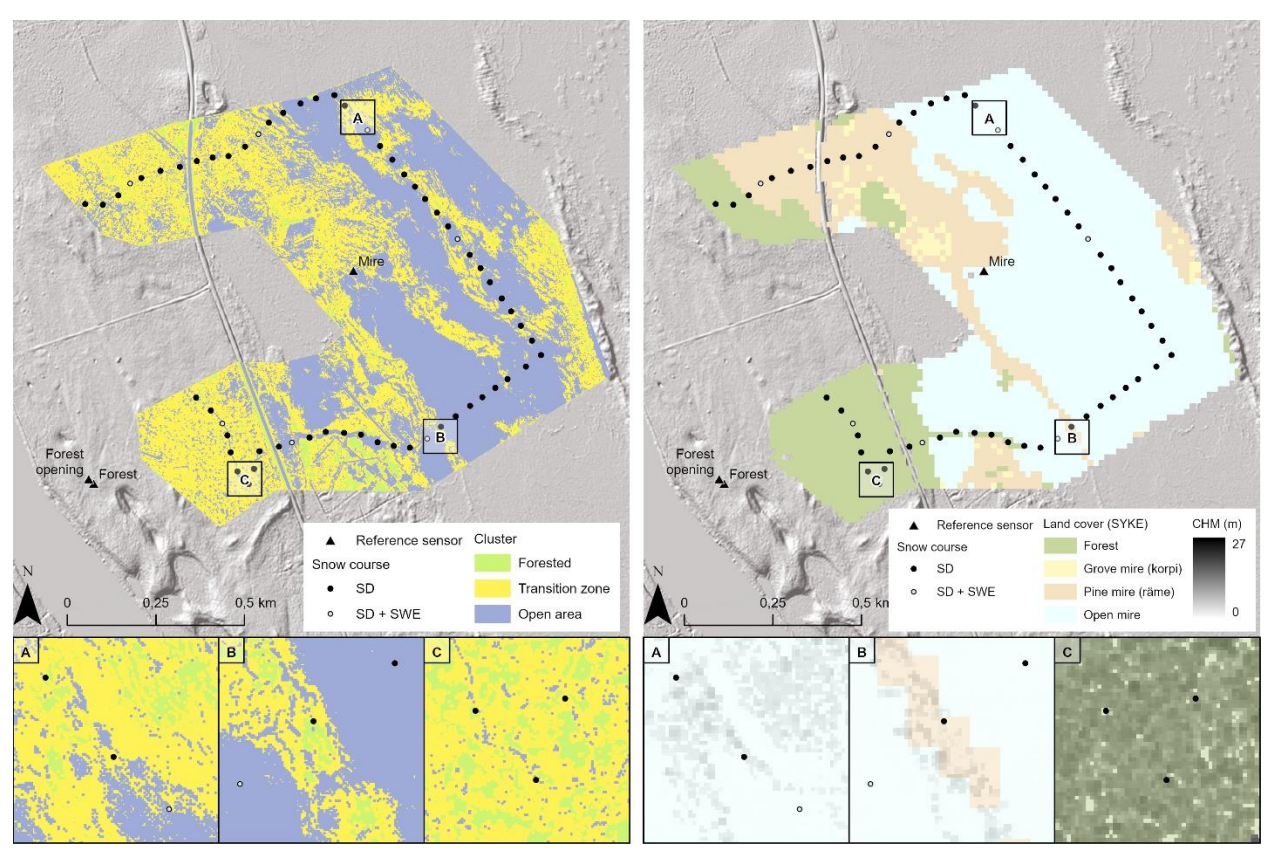


Figure 3. Sodankylä site cluster and vegetation characteristics. Bounding boxes A, B and C are examples of different cluster zones in relation to their canopy height and land cover.

Table 4. Cluster characteristics in relation to the entire study area of both sites

375

380

Site	Sodankylä			Pallas	Pallas		
Cluster	1	2	3	1	2	3	
Frequency %	21	45	34	32	42	26	
Mineral soil (forests) %	29	25	6	78	58	55	
Grove mire (korpi) %	3	2	1	2	4	2	
Pine mire (räme) %	49	19	5	17	18	9	
Open mire (avosuo) %	20	54	87	3	20	33	
CHM (m) mean	4.6	4.7	1.8	4.3	6.2	7.5	
Distance to forest (m) mean	1	3	14	1	2	7.5	
Max modelled snow depth (cm)	75	70	59	111	106	103	
Max modelled SWE (mm)	164	147	114	267	247	234	

Cluster 2 is the most common, covering 45% of the total area, and is primarily located in the transition zone between forest and open areas, including forest gaps, mire edges, and forest-mire boundaries (Fig. 3). This cluster has a mean canopy height of 4.7 m and is on average 3 meters away from cells classified as forests (Table 4). The modelled peak snow depth occured on 14.3.2024 (70 cm) and SWE on 23.4.2024 at 147 mm (Table 4). Snow course measurements that are classified as cluster 2 have their snow depth peaking on 15.3.2024 with an average of 67 cm, and SWE on 24.4.2024, with an average of 166 mm (Fig. S2, supplementary material).

Cluster 3 predominantly occurs in open areas with a low canopy height, with 87% of the area classified as open mire. This cluster consistently exhibits the lowest snow depths and SWE values compared to the others (Fig. S2, supplementary material). The highest modelled snow depth and SWE values for cluster 3 are at the same time as for other clusters, snow depth peaking on 14.3.2024 (59 cm) and 23.4.2024 (114 mm). The snow course snow depths and SWE from cluster 3 both peaked on 15.3.2024 with an average snow depth of 57 cm and SWE of 138 mm.

3.2.2 Pallas snow depth and SWE clusters

385

390

395

400

415

420

In Pallas, the three clusters derived from snow depth maps show similar characteristics to those in Sodankylä (Table 4). The more common cluster 2 covers 42% of the study area, with cluster 1 covering 32% and cluster 3, as the smallest, covering 26% of the area. The snow depth in the Pallas snow course began to decrease as early as late February across all clusters (Fig. S3, supplementary material). This decline was less pronounced in points classified as cluster 1 compared to the other two clusters. However, the timing of peak SWE, marking the onset of snowmelt, was later in the spring compared with snow depth and varied among the clusters.

Cluster 1 is predominantly located in the forested areas, which accounts for 78% of the cluster, while the open areas cover only 3% (Table 4). The mean canopy height is approximately 4.3m and the distance to the forest cells is less than 1m, which is less than in other groups, suggesting smaller and denser forest types. Until January, the modelled snow depths for cluster 1 followed similar snow depths to the other clusters, but after February they surpassed those of other clusters and remain the highest until the end of the season (Fig. S2, supplementary material). Changes in the snow depths between February and March were small, with occasional fluctuations. The modelled snow depth of cluster 1 peaked on 28.3.2024 (111 cm) and the SWE peaks on 10.5.2024 with SWE of 267 mm. Snow measurements from the snow course show that points classified to this cluster had their peaks in snow depth on 22.2.2024 and 25.4.2024 with both having an average snow depth of 102 cm and SWE on 25.4.2024 with 265 mm.

Cluster 2, identified as a transition zone, is typically located near forest edges, forest openings and small-scale open mire areas (Fig. 4). Forested areas cover 58% of the cluster, while open mire areas contribute 20%. The mean canopy height is approximately 6m with a 2.2m distance from the forest edges (Table 4). The snow depth patterns for this cluster align with those of other clusters until late February, after which the snow depths in cluster 2 started to decrease. The modelled snow depth peaked in mid-March on 18.3.2024 with 106 cm, but also on 17.2.2024 with 105 cm. The modelled SWE peaked later, on 28.4.204 at 247 mm and on 10.5.2024 with a SWE of 248 mm. The results are similar to the manual snow course measurements, where points classified to this cluster had their snow depth peak on 22.2.2024 (101 cm). However, snow course SWE peaked twice, having an average of 227 mm on 27.3.2024 and 233 mm on 25.4.2024.

Cluster 3 covers 26% of the Pallas area and is marked by a mixture of forest (55%) and open mire (33%) environments (Fig. 4). It has the greatest distance from forest cells and the tallest mean canopy height of 7.5 m (Table 4). This cluster is typically found in open mires or high canopy forests. Modelled snow depths in cluster 3 were initially the highest at the start of the season but exhibited a lower rate of increase compared to the other clusters after January and remained the lowest throughout the rest of the season (Fig. S3, supplementary material). The peak modelled snow depth, 103 cm, occurred in late February, 17.2.2024, after which the snow depth steadily declined. The modelled SWE peak was at the same time as for cluster 2, on 28.4.2024 (237 mm). Snow course snow depth measurements were the highest on 22.2.2024 with an average of 96 cm. SWE measurements from the snow course within this cluster are limited, with only five measurements taken during the melting period in late April and early May. During this period, SWE values were initially low but peaked at 186 mm on 7.5.2024 (Fig. S3, supplementary material).

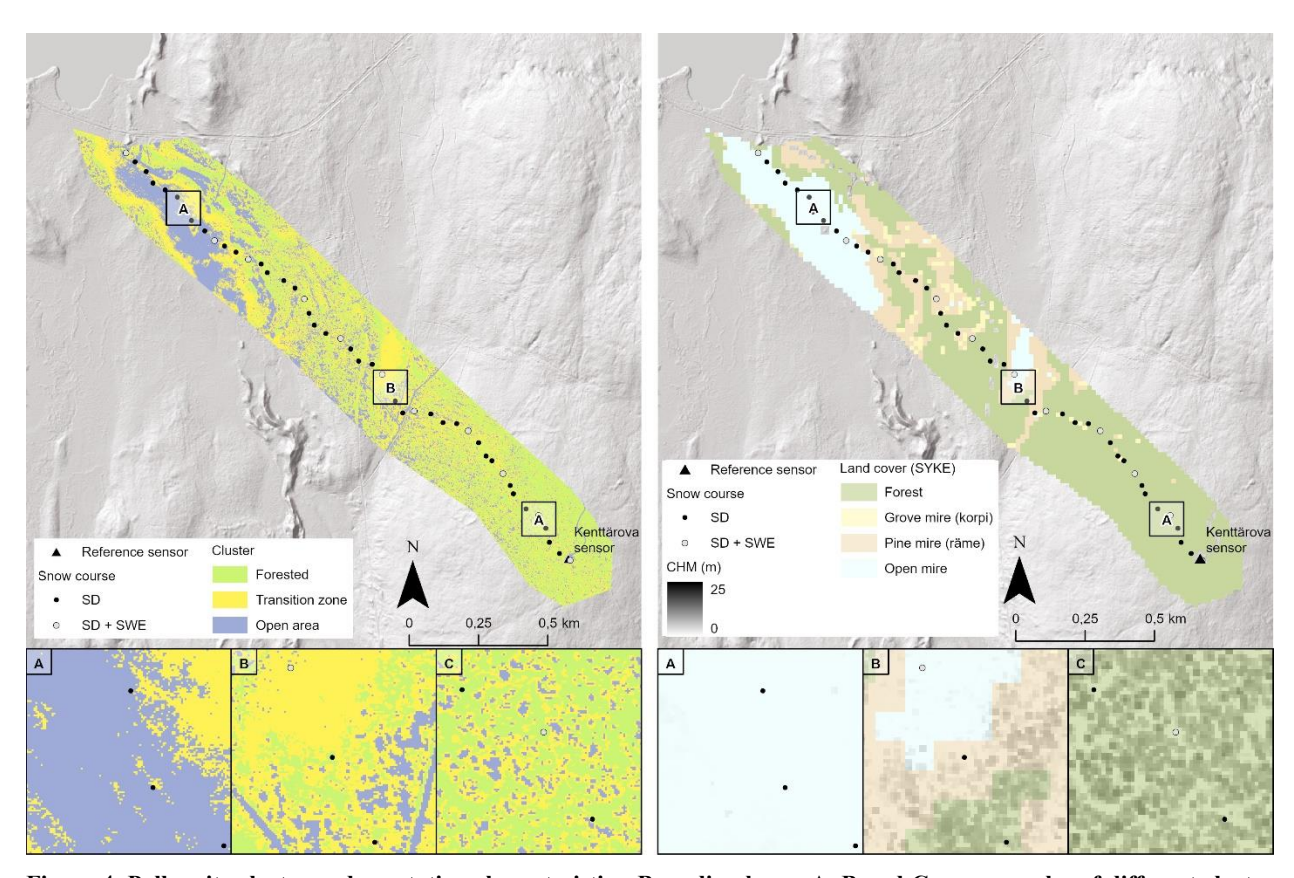


Figure 4. Pallas site cluster and vegetation characteristics. Bounding boxes A, B and C are examples of different cluster zones in relation to their vegetation.

3.2.4 UAV accuracy in comparison to clusters

430

435

To evaluate the accuracy of LiDAR-UAV snow depth by cluster in relation to the representativeness of reference snow depth sensors, SD measurements taken during the snow course were assigned to their representative cluster. When comparing the UAV-based LiDAR SD maps and manual snow course SD measurements, the LiDAR maps consistently underestimate the snow course measurements in both Pallas and Sodankylä (Fig. 5a, 5b). In Sodankylä, all snow course measurement campaigns show similar correspondence to the LiDAR snow depth maps and variations among clusters are similar, showing consistent agreement with snow course measurements (Fig. 5a). In Pallas the snow course measurements classified as cluster 1 correspond the best to the LiDAR snow depth maps, while the largest discrepancies are observed in cluster 3, typically located in wet mire areas (Fig. 5b). The accuracy of UAV LiDAR maps decreases towards the melting season, where, especially in Pallas, the SD estimates are on average up to -30 cm of the snow course measurements.

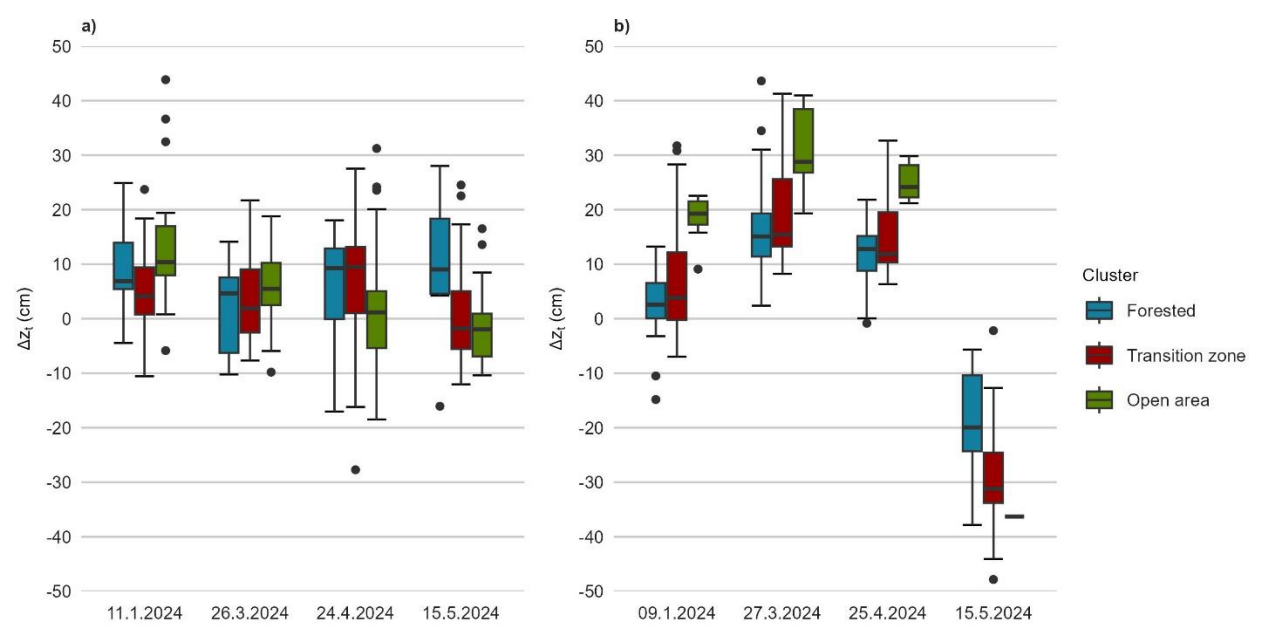


Figure 5. Differences in Δz_t (cm) between the UAV-based LiDAR snow depths and snow course measurements by each campaign and representative cluster in (a) Sodankylä and (b) Pallas.

450

Snow course measurements and the UAV-based LiDAR snow depth maps for each campaign were compared with the reference snow depth sensor measurements of the study area (Fig. 1; Fig. 2) to define the overall representativeness of the measurements and clusters. In Sodankylä, all the aforementioned datasets follow similar patterns: Clusters had similar mean snow depths as the sensors and were within the ranges of snow course measurements (Fig. 6a), except in May, when the snow course snow depths did not match UAV LiDAR nor the sensor snow depths. The highest snow depths were in forested cluster, and the reference sensor located in the forest opening. In Pallas, the UAV LiDAR snow depth maps underestimate the snow height in relation to both snow course measurements and reference snow measurement (Fig. 6b). Cluster 1 has the highest correspondence to the snow course and reference sensor compared to the areas classified as other clusters.

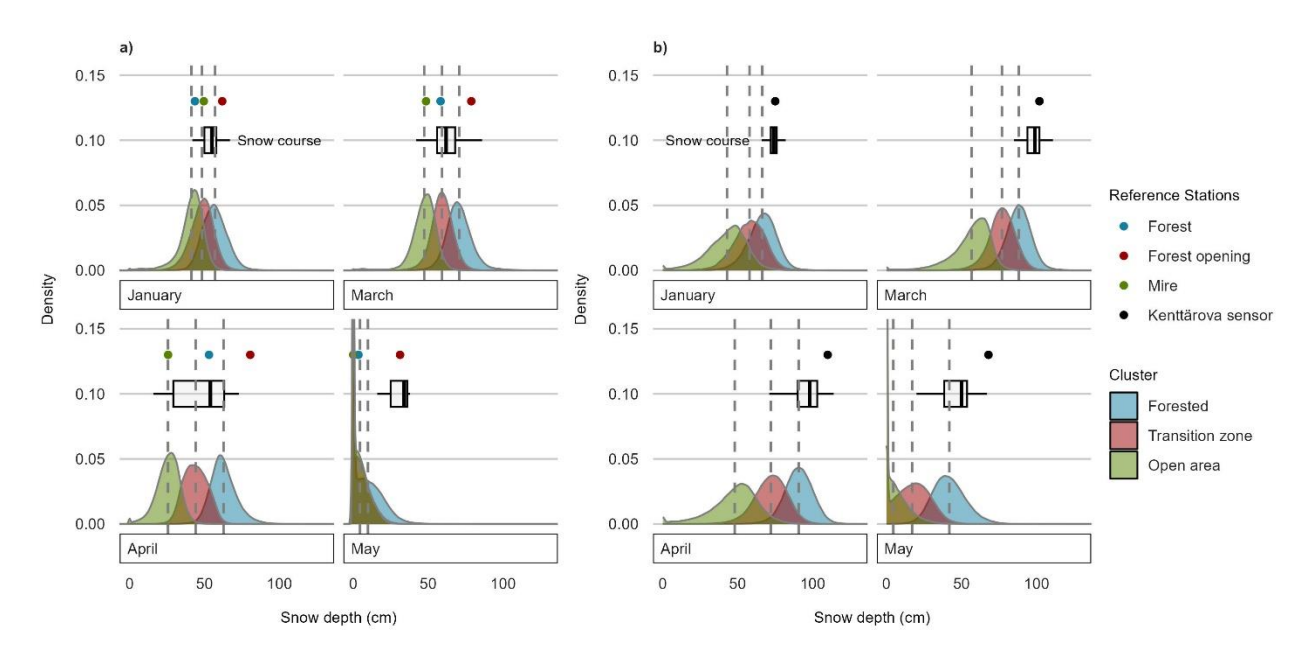


Figure 6. Reference sensor snow depths compared to UAV LiDAR snow depths by cluster in Sodankylä (a) and Pallas (b) in each campaign. Dashed lines are the mean values of snow depths at each cluster.

3.3 Model validation

455

460

465

470

3.3.1 Comparison of modelling results to snow course data

The model creates daily snow depth and SWE estimates for the two study sites. These estimates were compared to the snow course measurements and UAV LiDAR snow depth maps to estimate their accuracy (Table 5). The snow depth predictions of modelled maps have an overall accuracy of 8.0 cm in Sodankylä and 5.8 cm in Pallas compared to the manual snow course measurements (Table 5). The SWE values differ from snow course measurements in Pallas, with RMSE of 35.6 mm and 33.1 mm in Sodankylä during all measurements in winter 2023-2024. The predicted SWE values of the Sodankylä snow course follow the observed snow course SWE values (Fig. 7a). The model tends to slightly underestimate the SWE, particularly during the late season, but the median values of measurements fall within the model's predictive range. Model performance is the highest in February, with RMSE of 12 mm (n=7). In contrast, the performance declines towards the end of the season with RMSE of 73 mm in May (n=4), as can be seen in table 7.1.

In Pallas, the modelled SWE values are typically within the range of manual SWE measurement values (Fig. 7b). The model has an overall accuracy of 32 mm (Table 5), with its best performance observed early in the season, with RMSE of 6 mm in November (n=12) and 8 mm in December (n=12), as shown in Table 5. The highest error, 59 mm (n=12), occurs during the onset of the rapid snowmelt in early May. Despite this, the modelled SWE values successfully capture the seasonal peak in April and May, consistent with the snow course measurements.

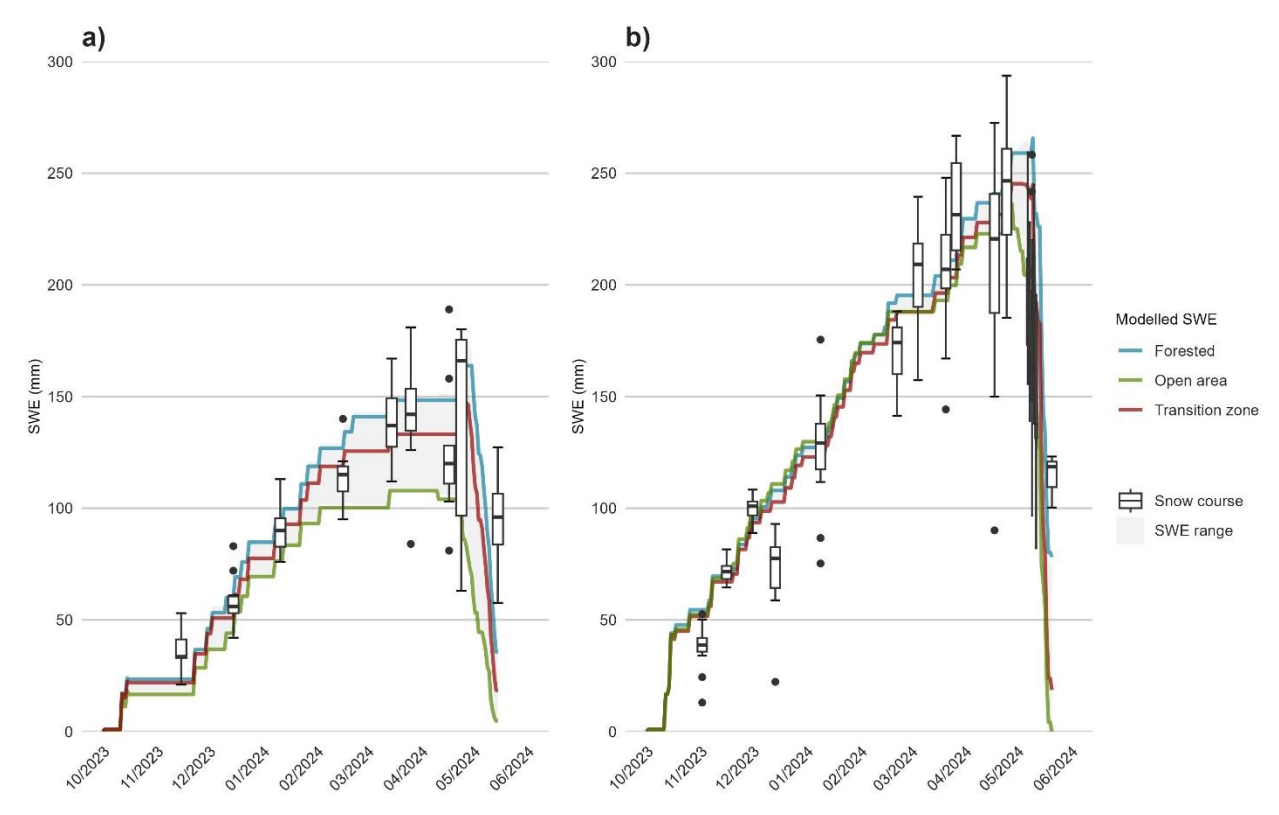


Figure 7. Modelled SWE values in comparison to measured SWE values of the snow course in Sodankylä (a) and Pallas (b) in 2023-2024.

Table 5. RMSE for Sodankylä and Pallas modelled SWE

Sodankylä			Pallas			
Date	RMSE SD (cm)	RMSE SWE (mm)	Date	RMSE SD (cm)	RMSE SWE (mm)	
15.11.2023	6.3 (n=62)	15 (n=7)	2.11.2023	4.5 (n =46)	18 (n=12)	
15.12.2023	5.9 (n=62)	13 (n=7)	16.11.2023	4.1 (n=46)	6 (n=12)	
11.1.2024	4.6 (n=62)	16 (n=7)	1.12.2023	3.9 (n=46)	8 (n=12)	
16.2.2024	5.0 (n=62)	12 (n=7)	14.12.2023	3.5 (n=46)	39 (n=12)	
15.3.2024	6.4 (n=62)	30 (n=7)	9.1.2024	4.1 (n=45)	25 (n=12)	
26.3.2024	6.7 (n=62)	32 (n=7)	22.2.2024	4.7 (n=45)	26 (n=12)	
17.4.2024	9.2 (n=60)	37 (n=6)	5.3.2024	5.2 (n=46)	26 (n=12)	
24.4.2024	13.8 (n=62)	50 (n=6)	21.3.2024	5.5 (n=46)	24 (n=12)	
15.5.2024	9.7 (n=62)	73 (n=4)	27.3.2024	4.8 (n=46)	34 (n=11)	
Mean	8.0 (n=555)	33.1 (n=58)	18.4.2024	6.3 (n=45)	53 (n=12)	
			25.4.2024	6.4 (n=45)	26 (n=12)	
			4.5.2024	6.7 (n=46)	59 (n=12)	
			7.5.2024	6.3 (n=46)	67 (n=12)	
			15.5.2024	8.1 (n=38)	25 (n=11)	
			21.5.2024	9.3 (n=46)	29 (n=3)	
			Mean	5.8 (n=677)	35.6 (n=169)	

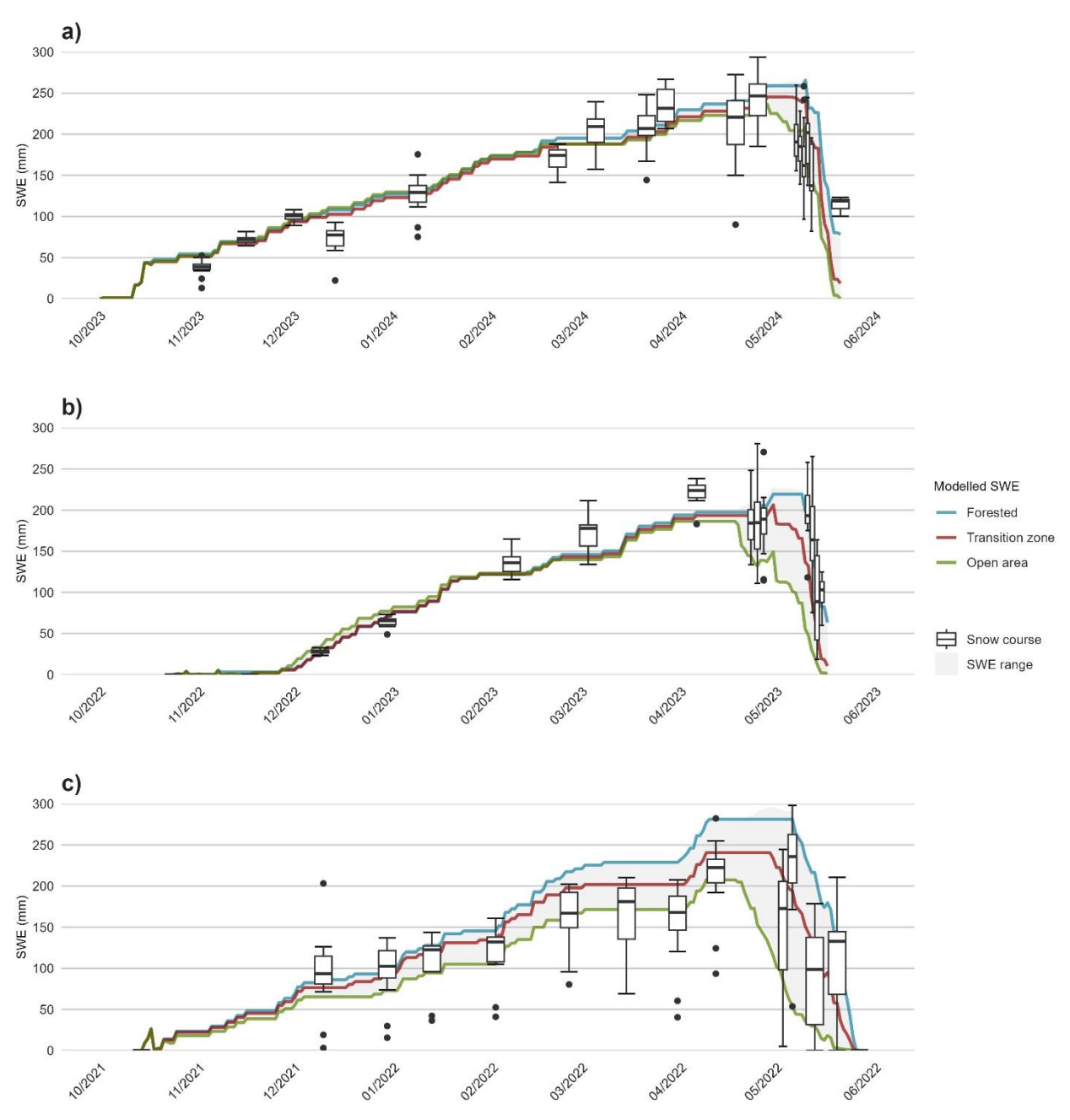


Figure 8. Modelled SWE of the previous winters, (a) 2023-2024, (b) 2022-2023 and (c) 2021-2022, at Pallas in comparison to the snow course SWE measurements.

485

ClustSnow-derived clusters therefore served as a valid extrapolation basis for snow depth and SWE measurements throughout the entire snow season 2023-24. Previous application of ClustSnow suggests that these clusters are not only suited to extrapolate measurements of the same season in which the cluster's underlying snow depth maps were acquired, but are instead transferable to other snow seasons (Geissler et al. 2024). Clusters defined by this study's snow dataset of 2023-2024 were therefore used to see how well the model can reproduce previous years' snow course measurements. SWE measurements from previous years are available for Pallas starting from 2021, although the number of measurements varies across years. The results show that SWE values from the winter 2022-2023 snow course are aligned with model estimates, also capturing the peak SWE in late April (Fig. 8b). The winter of 2021–2022 exhibits the greatest variability in snowline SWE measurements, with the model overestimating SWE for most

of that winter. In other winters, the model typically underestimates SWE relative to snow course measurements.

Additionally, the variance in SWE values across clusters is largest during the winter of 2021–2022, reflecting greater variability in snow depth along the snow course. However, the average of the SWE from the snow course in winter 2021-2022 aligns with cluster 3, and ClustSnow successfully captures the SWE peak at the beginning of May 2022. The model generally captures the snow course median SWE values from the manual measurements, and the peak SWE values and their timing in previous winters.

3.3.2. Spatial accuracy of the model is influenced by spring floods and snow wind distribution

495

500

505

Figure 9 visualizes the modeled snow depths for the March campaign in Sodankylä, highlighting the influence of clustering on snow depth predictions. The modeled snow depths align with the observed snow course measurements, but the model struggles to accurately represent extreme high or low values of snow depths captured by the UAV LiDAR. The figure also demonstrates the effect of adding more clusters to the model. For example, 6 clusters would provide more detailed snow depth estimates, but would still miss the actual variability of the snow depths. The UAV LiDAR shows the spatial variability in snow depth between snow course measurement points, which are not captured during the snow course measurement survey. To be able to evaluate the model performance spatially, comparisons between modelled snow depth maps and UAV LiDAR maps were conducted for each of the campaigns. First, the difference between the UAV LiDAR SD map and the model SD output was derived (Fig. 10 & 11); the differences were then squared, averaged and the square root of the mean was calculated to obtain overall RMSE for the campaign and model.

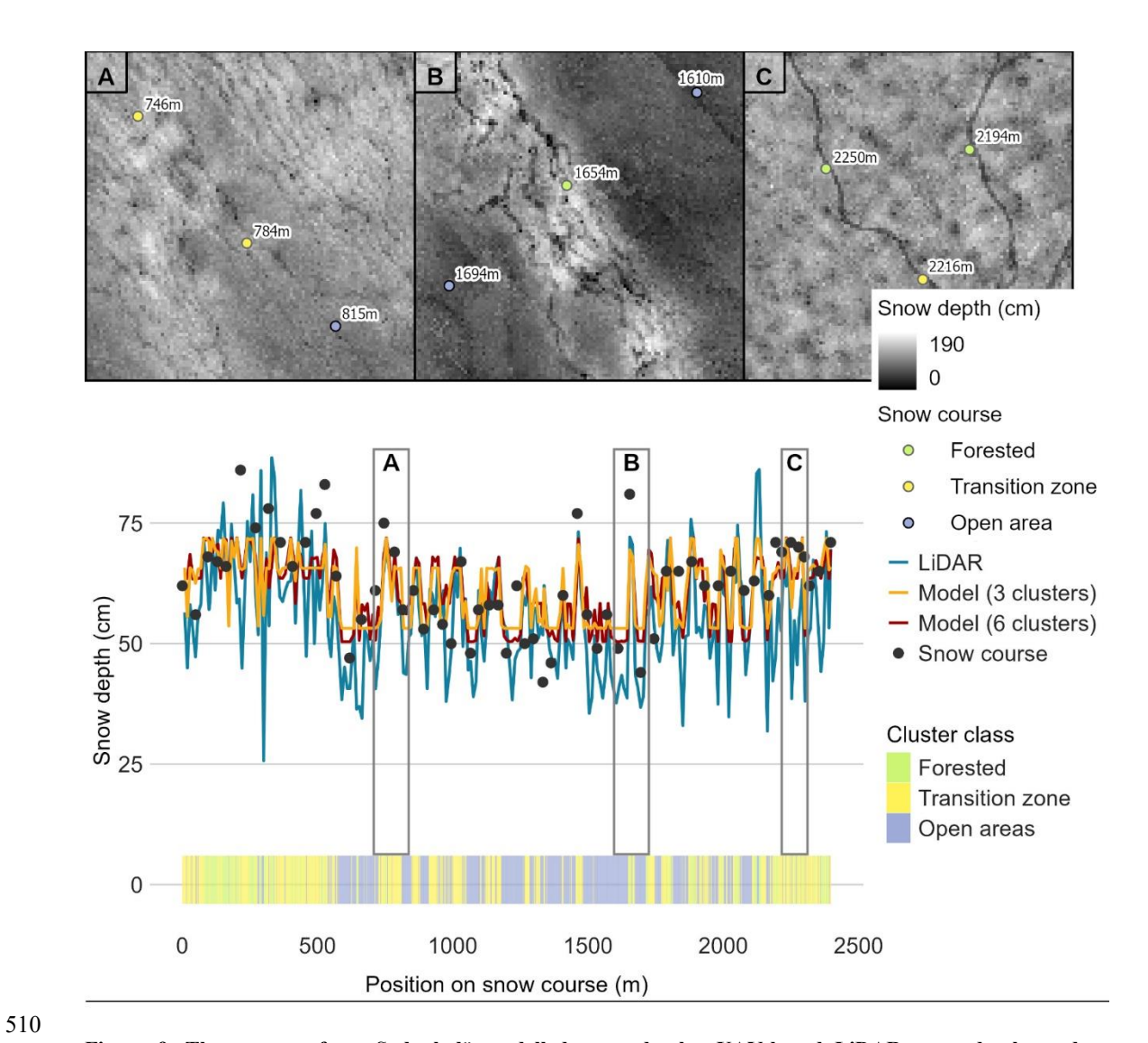


Figure 9. The transect from Sodankylä modelled snow depths, UAV-based LiDAR snow depths and snow course measurements and their representative clusters on 26.3.2024. The yellow line shows the model output of the model with the number of clusters set to three, as used in this study. For comparisons, the red line represents the model output with the numbers of clusters set to six.

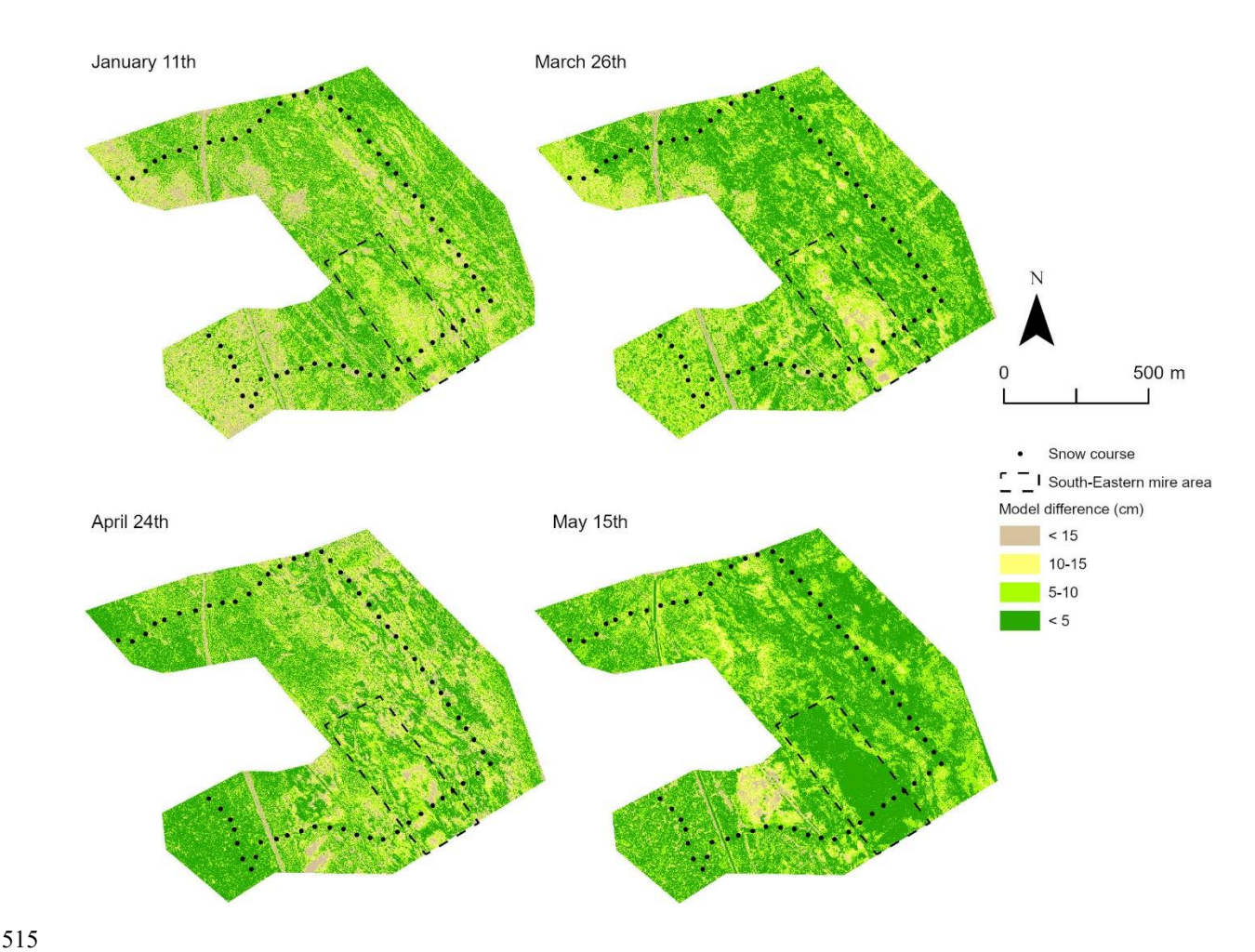


Figure 10. Sodankylä model performance from different UAV LiDAR campaigns. The values define the absolute difference between LiDAR based snow depth maps and the modelled snow depth maps.

In Sodankylä, the analysis resulted in RMSEs varying from 6.2 cm to 11.0cm (January: 11.0 cm; March 8.2 cm; April; 8.8cm; May 6.2cm). The accuracy of the modeled snow depth maps is influenced more by the timing of the campaign than by the specific location (Fig. 10). For instance, in an open mire area located in the southeastern section of the snow course, the model's performance varies significantly, with difference ranging from 10–15 cm in March, decreasing to less than 5 cm in May (Fig. 10, dashed box). Similarly, in the spruce dominated forest situated in the southwestern part of the area, the highest accuracy is observed in April (difference < 5 cm), whereas in January, the model predictions exhibit a larger discrepancy, with errors ranging from 10–15 cm.

520

525

530

In Pallas, the model has higher inaccuracies compared to Sodankylä, with RMSEs varying from 18.7 cm to 24.7 cm (January: 22.4 cm; March 24.7 cm; April 22.7 cm; and May 18.7 cm). The model therefore performs best at the beginning and at the end of the season. Spatially the model performs best particularly at the southern end of the snow course, characterized by homogeneous pine and mixed forest (Fig. 11). In contrast, the model has the highest errors in the broad Lompolonjänkä mire area in the northeast, where the snow is on top of a flooding mire area, and on the northern slopes of the bordering drumlins, where wind-driven snow accumulation is common. In these areas, the model estimates over 30 cm difference to the UAV LiDAR map.

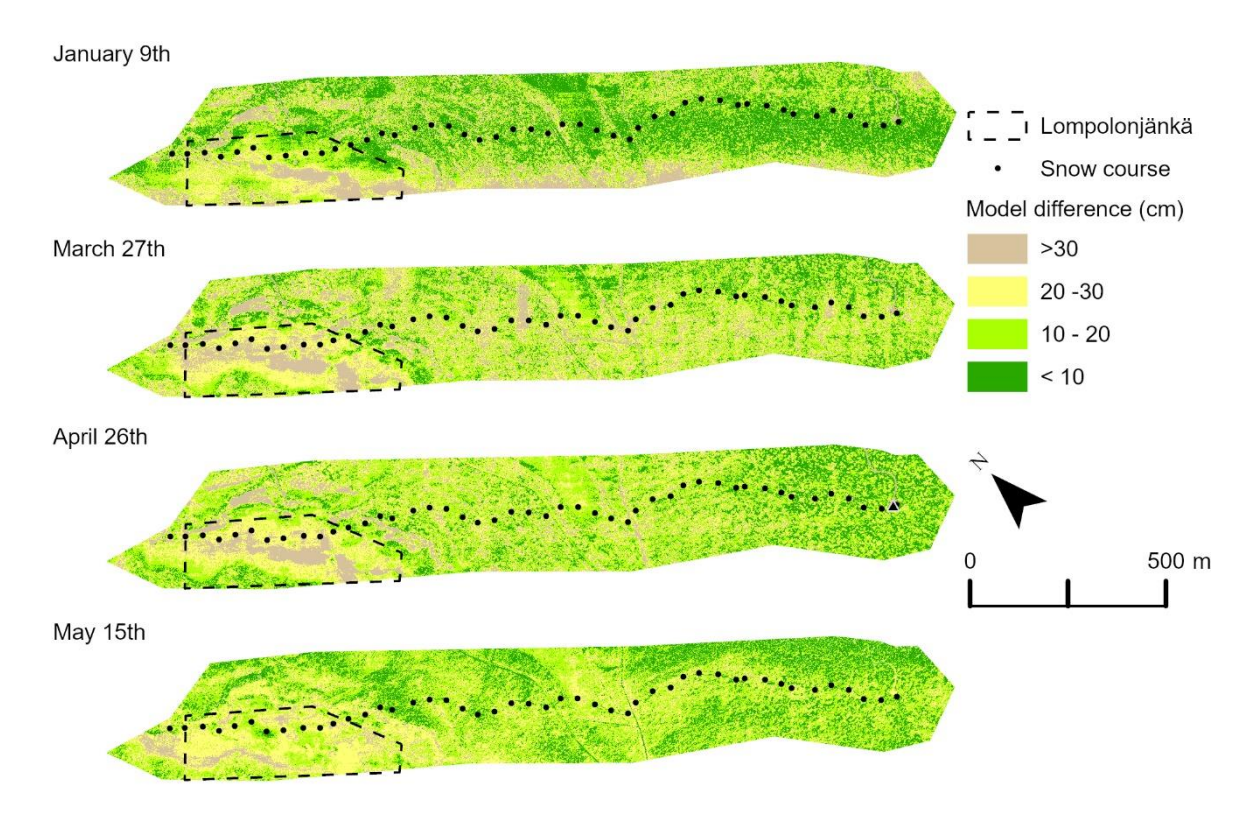


Figure 11. Pallas model performance from different UAV LiDAR campaigns. The values define the absolute difference between UAV LiDAR snow depth maps and the model output.

4 Discussion

535

540

545

550

555

4.1. Snow and ice conditions impacted UAV LiDAR accuracy

UAV LiDAR mapping showed high accuracy in all study sites and conditions, with the average RMSE of UAV LiDAR DTMs being 11.2 cm and 5.3 cm for Sodankylä and Pallas, respectively. These results align with previous studies, which have reported RMSE values from snow depth maps ranging from 9 to 17 cm (Dharmadasa et al., 2022; Geissler et al., 2023; Harder et al., 2020; Jacobs et al., 2021). However, our larger uncertainty and lesser accuracy was noted especially in the late melting period with flooding conditions, whichmight be impacted by laser beams reflection from water bodies.

The trueness of the snow depth maps derived from DTM maps varies between 0.9-13 cm and RMSEs of individual DTMs vary between 1 and 7 cm (excluding an outlier in Sodankylä, May 22.1 cm). The precisions here are based on the 5 GCP measurements suggested by Dharmadasa et al. (2022). Pallas has the most stable conditions and Sodankylä has the actual lowest bias in April (0.9 cm). The accuracy of the GCP location measurement itself can affect the accuracy estimates. For example, one measurement in Sodankylä (May) shows a significant difference to DTM, which decreases the overall accuracy of the site. The point was not excluded from the calculations, as the error may also be due to the DTM calculation errors from flooding areas. The accuracy of UAV LiDAR snow depth mapping is dependent on several factors, which can be divided into boresight errors, navigational errors, terrain- and vegetation-based errors, and post-processing-errors (Deems et al., 2013; Pilarska et al., 2016). For example, fallen tree trunks, very dense undergrowth or flooded marshes can pose challenges to point cloud classification and affect the output DTM quality (Deems et al., 2013; Evans & Hudak, 2007). Similarly, vegetation and terrain affect the accuracy of manual snow depth measurements.

The best accuracy of snow depth maps (0.9 cm) of all sites and campaigns was calculated from April campaign in Sodankylä. Two days prior to the flight campaign, on 24.4.2024, approximately 10 cm of new snow had fallen in the area, which helped to smooth the snow surface and to cover previously melted or frozen areas under the snow, positively affecting the LiDAR signal and hence the accuracy of the terrain model. In contrast, the trueness of snow depth maps in all sites is lowest in May (Table 3). Our findings highlighted increased measurement inaccuracies during that period, possibly because most of the snow had already melted and large areas were covered with slush and smooth water surfaces. This posed challenges for the DTM algorithm lowest Z-value obtained in cell, meaning that the height of the reflected laser beams in the water mass also affects the DTM elevations. The trueness values, on the other hand, are based on GCP plates placed in the area, which were located on top of the remaining snow. When the snow is surrounded by water, the model may be inaccurate and produce lower accuracy DTMs than when the surface is completely covered by either snow or thawed ground. To our knowledge, there is no systematical review on wet snow affecting laser beams. However, water generally has a low reflectivity in the infrared wavelength range compared to solid surfaces, and the return signal detected by the sensor is influenced by factors such as incidence angle and surface roughness (Fernandez-Diaz et al., 2014; Paul et al., 2020). These factors likely contributed to reduced accuracies of the surface detection in areas with localised open water during the melting season. The phenomenon can be seen especially in Sodankylä, which has the largest, typically flooding, mire areas among sites. Results were similar for Rauhala et al. (2023), where the poorest accuracy of SfM method based DTMs were collected during the late melting period in flooding areas. This is due to the manual snow course measurements, where these flooding points are marked as having zero snow depth and LiDAR-derived snow depth maps still showing snow in these areas. Some vegetation types, such as dense coniferous forests, are known to decrease the accuracy of different UAV methods of snow depth mapping (i.e Dharmadasa et al., 2022; Rauhala et al., 2023), as coniferous canopy reduce or even prevents ground returns. If we expect cluster 1 to present forested regions and cluster 3 to present open areas with low vegetation and compare the snow depth map accuracies to snow course measurements, we cannot distinguish similar phenomena in Sodankylä or Pallas (Fig. 5). On both sites, the best correspondence between snow course measurements and UAV LiDAR maps are in cluster 2, in forest openings. In contrast, especially in Pallas, the biggest disparities occurred in cluster 3. This may be due to snow course measurement poles lifting from the ground especially in wet areas where ground freezing and thawing move the pole over time.

Broxton & van Leeuwen (2020) recommended the SfM method for snow depth monitoring under certain conditions, such as in gently sloping terrains and areas without dense forest cover. The UAV LiDAR method was selected over the SfM method for this study due to existing dense forest canopy and frequent light conditions that would not allow reliable SfM data acquistion (Rauhala et al., 2023; Revuelto et al., 2021). With advancements in SfM camera technology, the SfM method could complement LiDAR monitoring, particularly in relatively flat regions like Sodankylä and Pallas. Nevertheless, challenges remain for both methods in large mire areas. While the SfM struggles with surface homogeneity, LiDAR faces accuracy issues in detecting bare ground under flooded, uneven and wet surfaces. Additionally, manual snow depth measurements are also less accurate due to ice and water layers on the ground.

4.2 Site characteristics explaining the different snow depth clusters

560

565

570

575

580

585

590

595

600

Vegetation and topography impacted snow depth clustering in our boreal and sub-arctic sites. Specifically, we noted that canopy cover, open peatlands and transition zones with wind shelter had a clear and similar influence on obtained clusters at both sites. Additionally, we noted that the clusters have similar snow dynamics in both sites. The number of clusters has a major impact on the performance of the clustering and ClustSnow and how determined clusters relate to the site's vegetation and topography characteristics.

This study applied ClustSnow with the number of clusters set to three, as initial tests demonstrated their suitability for representing different snow patterns in study areas and three clusters enable us to relate the snow depth patterns to

605 vegetational patterns. an equal number of clusters provides a basis for site comparability between the two study sites. Our analysis resulted in snow depth classification for forests with different trunk heights (cluster 1); transition zones between forests and open areas, including forest edges and gaps (cluster 2); and open areas (cluster 3), mainly peatlands. The results are consistent with those of Mazzotti et al. (2023) who noted that snow accumulation patterns can be classified into three groups, based on the relationship between canopy structure and ablation rate. However, as 610 also noted by Geissler et al. (2024), increasing the number of clusters could, in some cases, improve the accuracy of the end products and increasing the number of clusters would allow more detailed description of the snow patterns, as can also be seen in Figure 9. The sensitivity analysis performed for this study's sites confirm this assumtion. We found that the highest accruacies of the ClustSnow-derived snow products, evaluated against manual measurements, can be expected with the number of clusters set to six. Especially when the study area has high elevational differences or has 615 various topographical apects, more clusters would better correspond to the depth patterns. The most uncertainties related to the model parametrization of both models, the ClustSnow and Δsnow model, are due to the number of clusters (Fig 1., see appendices).

In forested areas, distinguishing between clusters 1 and 2 remains challenging due to their similar site characteristics (Tables 5 & 6). Forested areas present challenges for clustering because of varying snow height and dynamics influenced by canopy cover and trunk size (L.-J. Meriö et al., 2023). Forest gaps in the coniferous forests are known to create clear and distinct variations in snow depth within the forests, and SWE varies up to three times more in unevenly distributed forests compared to evenly distributed forests (Woods et al., 2006). For this reason, forested areas contained both clusters 1 and 2 in both sites. Cluster 1 receives the most snow and has the highest SWE values, especially during the late winter (Fig. 7a; 7b). Lundquist et al. (2013) concluded that this is the typical situation in cold climates, where snow lasts longer in forests than in forest openings. In both of our sites, snowmelt starts latest and snow cover last longest in cluster 1. The forested areas in Sodankylä and Pallas are spruce dominated, where the canopy shades the ground from sun radiation, reduces wind effects and traps snow, but also limits snowfall reaching the ground. In this cluster, we expect snow accumulation to follow canopy structure throughout the season and the ablation to be too slow or constant to change it, as defined by Mazzotti et al. (2023).

620

625

630

635

640

645

650

Cluster 2 is the most common cluster on both sites (Tables 5 & 6), likely since it can be found in both forested and open environments. While the snow depth trends across cluster 1 and cluster 2 are similar, cluster 2 experiences an earlier start of snowmelt in spring compared to forested cluster 1 (Fig. 7a; 7b). This indicates more short-wave solar radiation exposure compared to cluster 1, where SWE peaks at the end of April before the melting begins. Cluster 2 characteristics correspond to previous studies, by Koutantou et al. (2022) and Meriö et al. (2023), where canopy structure influences snow accumulation, but in ablation subsequently disrupts these patterns, resulting in earlier timing of snow loss. This can also be seen in the modeling outputs from the previous two winters in Pallas (Fig. 8), especially in winter 2022-23, when snowmelt in cluster 2 started simultaneously with cluster 3. These characteristics are seen in both sites and support the location of the cluster 2 as being in transition zones between open and forested areas.

Open areas are subject to wind redistribution and prolonged solar exposure resulting in lower and smoother snow depth patterns, corresponding with the results of cluster 3. In cluster 3, snow depth starts decreasing notably earlier than other clusters, in February 2024, suggesting faster melting due to both higher solar radiation and flooding. In the flooding mire areas, melting waters from below also accelerate snowmelt. Both snow depth and SWE values are lower in this cluster in comparison to other clusters, corresponding with results from L.-J. Meriö et al. (2023). An interesting aspect of the classification is the differentiation between the mires Lompolonjänkä (box A; Fig. 4) and Välisuo (box B; Fig. 4). Välisuo mire, classified to cluster 2, is more sheltered, surrounded by forests and is located at a higher altitude than the Lompolonjänkä mire, which is classified as cluster 3. Välisuo is drier and partly artificially drained, while Lompolonjänkä is drained by a small natural stream, typically flooding in spring (Marttila et al., 2021).

The clustering results support the results of other studies on snow distribution in boreal and sub-arctic sites. They also support the ability of the ClustSnow ability to model various environments and sites, both in Alps and the Arctic

boreal zone. Moreover, the results suggest that ClustSnow is generally transferable to large sites as well as to the arctic boreal climate. In a recent study from the Pallas site by L.-J. Meriö et al. (2023), the variations in snow depth were partially explained by canopy interception, longwave radiation emitted by trees, and wind-driven redistribution, which contributed to snow deposition along forest edges in both forested and peatland environments. The snow depth was higher within dense canopy, with the greatest accumulation observed in coniferous forest areas, followed by mixed forests, transitional forest/shrubland, and open peatlands. In both Sodankylä and Pallas the dominant winter wind direction is from the south, which leads to snow accumulation in forest canopy and their leeward side, where typically the highest snow depths are measured, corresponding to the results from Dharmadasa et al. (2023). In Pallas this results in snow accumulating particularly behind the drumlins north of the Lompolonjänkä mire (Fig. 4 Box A). This is also reflected in the accuracy of the model in these areas - the three clusters may not be sufficient to account for the particularly high snow depths of the northern sheltered slopes (Fig. 11). In comparison, snow dynamics in Sodankylä are influenced by vegetation rather than by topographical variations, as the area itself is flat with elevation differences of less than two meters. Forest structure is the main driver of snow accumulation, but short-wave radiation can disrupt these patterns, especially on south-facing slopes where there is expected to be more early-season ablation (Mazzotti et al., 2023). Weather further affects accumulation and ablation processes, leading to interannual variations in snow distribution, explaining why the relationship between snow distribution and canopy structure varies by location and year.

655

660

665

670

675

680

685

690

K-means clustering is widely used in many applications for partition datasets but is known to have problems associated with centroid initialization, handling outliers and dealing with various data types (Ahmed et al., 2020; Morissette & Chartier, 2013). While more clusters might be able to capture finer details, such as directional classes (Mazzotti et al., 2019), the three clusters obtained in this study corresponds to land-cover These results align with previous findings that emphasize the importance of canopy structure in addition to topography and weather conditions on snow dynamics (Dharmadasa et al., 2023; Mazzotti et al., 2023). For instance, Geissler et al (2023) classified their Alpine study area into four clusters, further subdividing the open cluster into shaded and exposed clusters. Although using more than three clusters could potentially improve finer scale spatial accuracy, as can be seen in Fig 9 and the number of clusters is always a question of data used and left to the user to decide, as noted in the study by Geissler et al. (2023). Based on our observations, together with the results of the study by Geissler et al. (2024), we conclude that the number of clusters is dependent on the landscape characteristics of the site and the purpose of the model output. If the interest is to investigate the differences between snow dynamics in different environments, we recommend increasing the cluster number to also include shaded, exposed and potentially different forest types to capture local variability (Currier & Lundquist, 2018; Fujihara et al., 2017; Mazzotti et al., 2020, 2023; Trujillo et al., 2007). Our sensitivity analysis also showed improvements in the snow products with more clusters. In areas with a larger variety of terrain types, such as diverse slopes and orientations, more categories (4 to 6) could be justified.

4.3 Lidar-based snow clustering and modeling produces SWE estimates comparable to snow surveys

The clustering derived from UAV LiDAR snow depth maps, combined with the Δ snow model, produced snow depth and SWE estimates with RMSEs of 8 cm and 33.1 mm in Sodankylä, and 5.8 cm and 35.6 mm in Pallas. The model can reproduce the onset of snowmelt and peak SWE and, after one season of drone surveys, needs only daily snow depth measurements as input. The localization of model parameters, especially pmax and $\rho\theta$, and the amount of daily snow depth reference data for the identified clusters, improved the results.

The results are consistent with a similar study by Geissler et al. (2023), where the model errors were 8 cm for snow depth and 35 mm for SWE in comparison to manual snow measurements. Winkler et al. (2021), the creators of the presented Δsnow model, produced a SWE RMSE value for their entire validation data set of about 30.8 mm, which is consistent with other similar models and the results obtained in this study. Multilayered thermodynamic one-dimensional models for SWE estimation, such as SNOWPACK, CROCUS and SNTHERM, obtained more accurate results in the Langlois et al. (2009) study with an RMSE of 12.5-14.5 mm, but these models also require atmospheric

variables that are not ubiquitously available. Studies with CROCUS also have produced SWE estimates RMSE values in the same order as this study (Vionnet et al., 2012) with an accuracy of 39.7 mm. Mortimer et al. (2020) studied the long-term gridded SWE products and compared their results to snow course measurements. None of the 9 tested products were significantly better than others, rather a multiproduct combination provided the most accurate results. The lowest RMSE in Finland was 33 mm, produced by ERA5. Thus, depending on the region and winter climatic conditions, there may be variability in the modelling results and our UAV results are in typical measurement estimate ranges.

705

725

730

735

740

745

The RMSE of the modelled snow depths (Table 5) in Sodankylä are higher than in Pallas, likely due to several factors. 710 The RMSEs were calculated in comparison to manual snow course measurements. In large mire areas, such as those found in Sodankylä, the formation of ice layers at the bottom of the snowpack may compromise the accuracy of snow course measurements (Stuefer et al., 2020). Additionally, the accuracy of snow depth maps in Sodankylä was reduced when parts of the areas were flooded in May (Table 3). Also, normalizing snow depths when generating daily estimates for clusters ensures internal consistency but reduces local variability, leading to an underestimation of extreme values. 715 Even though the RMSE of the modeled snow depths relative to snow course measurements in Pallas is lower than in Sodankylä, the RMSEs calculated for the entire study area are higher in Pallas. Specifically, RMSE values range from 18.7 to 24.7 cm in Pallas, compared to 6.2 to 11.0 cm in Sodankylä. One contributing factor to the higher RMSE in Pallas is the accuracy of the snow course measurements (Fig. 5). The errors arise from the use of interpolated snow course data as model input. These interpolations overestimate actual snow depths in Pallas (Fig. 6), introducing a systematic bias. This overestimation of snow course measurements also partially explains the higher RMSE of the 720 Pallas SWE model compared to Sodankylä, even though the modeled snow depth estimates for snow course were more accurate (Table 5). In contrast, UAV LiDAR-derived snow depths for the entire Sodankylä region closely align with snow course measurements (Fig. 6), indicating better agreement between manual measurements and broader regional snow depth estimates in this area.

The ClustSnow model can detect SWE peaks in some of the clusters (Fig. S2; S3, supplementary material). In Sodankylä, the SWE peak for cluster 2 aligns with the snow course measurements recorded at the dates between 22.4 and 24.4.2024. The model estimates SWE for cluster 3 to range between 107 and 114 mm from 14.3 to 23.4.2024 and the snow course data for the cluster 3 indicates that SWE reaches its peak in mid-March before gradually decreasing until the end of April, demonstrating good agreement with model estimates. However, while the timing of the peak is well captured, a slight discrepancy remains in its magnitude. Due to the limited number of snow course measurements classified within cluster 1, detecting meaningful correlations for this cluster was not possible. In Pallas, the model estimates SWE peaks for cluster 1 and 2 on 10.5.2024, while for cluster 33, the peak is predicted to occur earlier, on 28.4.2024. However, a slight temporal lag is observed as snow course measurements indicate that for clusters 1 and 2 the SWE peaks on 25.4.2024. For cluster 3, the discrepancy is more pronounced, with observed SWE peaking already at the end of March. The results show regional differences in SWE accumulation and melt dynamics, with the model capturing general trends but showing slight timing offsets, particularly in Pallas.

The model was validated at the Pallas site to assess its performance under different winter conditions from 2021 to 2023 from which no data was used in developing the model (Fig. 8). The results indicate that the model successfully captures both the peak SWE and its timing, despite variations in winter conditions between different years. During the 2021–2022 winter, the variance in both snow course SWE and modeled SWE is notably higher compared to the other winters. This increased variability is partly due to the fluctuating snow depths in that season caused by both midwinter melt events and heavy snowfall events.

Several studies predict increase in mixed and liquid precipitation in winter months in Finland and, particularly in northern parts, increased solid precipitation and earlier springs (Luomaranta et al., 2019; Ruosteenoja et al., 2020). Rain-on-snow (RoS) events are expected to increase in the future for the northern Norway region during spring and summer (Mooney & Li, 2021; Pall et al., 2019), potentially leading to an increase of such events in northern Finland

too. Such events increase the liquid water content of the snowpack, leading to rapid saturation and accelerated snowmelt, reducing snow depth faster than natural snowmelt processes (Yang et al., 2023). Even though Geissler et al. (2023) noticed the Δsnow model limited the capacity to map the SWE change during RoS events, the SWE estimations of this model add value to operational snow course measurements by enabling continuous monitoring of changes between monthly observations. This capability is especially valuable for capturing rapid changes during events such as snow depth variations caused by melting or snowfall, where these dynamics can be scaled across the entire study area rather than relying on data from a single reference sensor. By integrating daily estimates from local snow depth sensors with snow course data and clusters, our approach enhances event coverage in modeling. The model's ability to capture peak snow depth and melt-out dates in real time, provided that reference snow depth sensors transmit data online, offers essential data for hydrological observation networks and improves the spatiotemporal resolution of snow course measurements.

4.4 Practical aspects and suggestions for future studies

765

770

775

780

785

Snow monitoring data is essential for flood prediction, infrastructure management, forecasting hydropower production and for recreational use such as skiing. The forecasts derived from these data support river regulation and broader water management practices. In addition, daily observations are utilized by various stakeholders, including local businesses. These datasets also play a critical role in evaluating the impacts of climate change and informing the development and implementation of adaptation strategies. Integrating UAV-based snow depth surveys into established snow course areas—conducted over at least one winter season, and preferably across multiple years—can significantly enhance the spatial representation of snow depth estimates. By applying clustering techniques to these survey data within a region and validating the results against point-based snow course measurements, it is possible to upscale localized measurements and improve the spatial and temporal resolution of hydrological monitoring. This combination of observation-based clustering and high-resolution UAV data offers a promising approach for enhancing the monitoring of snow cover dynamics at both site-specific and regional scales. The outcomes of this study suggest that the applied ClustSnow workflow is transferable and could be effectively applied in other regions to support improved snow monitoring and water resource management.

This study applied intensive UAV LiDAR campaigns to capture fine detailed information on snowpack variability also in forested areas, which are known to reduce spatial coverage of UAV-based SfM methodology (Broxton & van Leeuwen, 2020), especially in poor lighting conditions and dense forest canopy cover (Rauhala et al., 2023; Revuelto et al., 2021). Regardless of the sensor used, the impact of winter conditions on the battery life of the drone should be considered. The batteries of the DJI Matrcie 300 RTK had to be replaced up to five times during the flight campaign, especially in cold weather. Occasionally RTK coverage can also become a limiting factor in remote areas, for example in Pallas in January, due to the temporary unavailability of the VRS signal. However, especially in sparsely vegetated areas, the UAV SfM method could offer a more cost-efficient method for producing 3D data on snow dynamics and support the output of more expensive UAV LiDAR. UAV data acquisition using LiDAR or SfM can also further support the spatiotemporal resolution of remote sensing products, as their usage in local scale snow research is still limited due to spatial and temporal coverage issues (Muhuri et al., 2021; Stillinger et al., 2023; Tsang et al., 2022b). As noted by Geissler et al. (2023), this method combines observations and machine learning and can improve spatial representation of hyper-resolution models (Mazzotti et al., 2021) or advance refining sub-grid variability in larger-scale models (Currier & Lundquist, 2018).

Mazzotti et al. (2023) indicated that the snow distribution patterns found at a specific location may not be consistent from year to year, especially in changing weather conditions. The snow distribution patterns are site-specific, based on vegetational and topographical differences, and some clusters might have different responses to different weather conditions. Winters with abnormal snowfall cause differences in snow extents and snow depth variability (Pflug & Lundquist, 2020). In our study areas, the winter of 2023–2024 was exceptional in terms of snow conditions. There were melt periods in the middle of winter, and spring seemed to arrive twice: first with a thaw in early April, and then snow melted completely in May. On average, there was also more snow than during a typical winter (Fig. 2), especially

in early winter. The model was developed based on these specific snow conditions, which means that winters with different characteristics may not align with the model's calculated clusters. This may partly explain, for example, the differences in SWE values for the winter of 2021–2022 (Fig. 8b). This winter also showed the greatest variation in measured SWE values, indicating larger homogeneity in snow conditions during that winter. A follow-up year with different weather conditions could enhance and verify the representativeness of the clusters and provide insights into interannual variability, as local snow distribution patterns show recurrent similarities (Sturm & Wagner, 2010).

Improvements in input data quality can enhance the accuracy of the model, but the model also seems robust. For example, improvements could be made to tackle Pallas site snow course measurement errors (Table 5). We would recommend a more comprehensive network of snow depth sensors that could improve daily snow depth forecasts based on snow course measurements, particularly in Pallas, where only limited data from the Kenttärova snow depth sensor is available. At least one reference sensor in each land cover type, corresponding to a cluster, would improve the estimates. As fresh snow density and maximum snow density are among the most important parameters of the model (Fontrodona-Bach et al., 2023), the model parameters should be localized for each site, rather than relying on estimates based on literature. Additionally, as the greatest inaccuracies in snow course measurements at Pallas were observed in mire areas, it is important to acknowledge that these regions are prone to greater errors in both manual and UAV-based snow depth data collection. Beyond the influence of snow-forest interactions, our results also emphasize the need to study snow accumulation and melt processes in extensive peatland areas, which are particularly prevalent in the Arctic boreal zone.

5. Conclusions

800

805

810

815

820

825

830

835

840

This work combines emerging methods in close-range remote sensing and machine learning for high spatial and temporal resolution estimates of snow depth and SWE. The work is an important new application of such methodology in the vast, yet relatively underexplored, boreal and sub-arctic snow regimes. The study conducted extensive field campaigns at two well-established snow and hydrology research sites, Sodankylä and Pallas in Finnish Lapland. The different sites represent different conditions, both in terms of topography and weather conditions. The snow depth maps from different areas and in different winter conditions are the first from these study areas at a centimeter scale of accuracy and allow an evaluation of the method in relation to other snow depth and SWE products.

The ClustSnow workflow applied in this study has the potential for the expansion of the current operational snow monitoring network to different sites. The resulting SWE and snow depth maps are possible to be produced in areas with snow depth sensors in different terrain types, or a regularly measured snow course with at least one snow depth sensor measuring daily. While the accuracy of the snow course measurements must be considered, the existing snow courses provide a good basis for similar approaches for local scale SWE and snow depth mapping in other boreal sites too. Though clusters formed here are based on only one winter and are site specific, we showed how they translate well to different winters with different snow amounts at the sites. Founded on the well-established consistency of local-scale snow distribution between years, the new technology applied in this research enables cost-effective solutions for SWE monitoring after one winter of UAV LiDAR surveys. Our work extends the previous applications of similar methods successfully to boreal taiga snow, where forests greatly complicate any snow monitoring, remote sensing or modeling.

With climate change leading to increasing temperatures, changes in precipitation regimes and more frequent rain-onsnow events, this methodology provides valuable tools for estimating rapid changes in snow depth and SWE at both local and catchment scales. Such spatially and temporally refined estimates of snowpack condition are needed for catchment scale snow model validation and calibration, as well as to improve resource planning and prediction.

Acknowledgements

We thank Joni Koivula (UOULU), Célestin Paquet, Markku Ahponen (FMI), Anna Kontu (FMI), Aleksi Rimali (FMI), and Mirka Hatanpää (Metsähallitus) for significant help with field sampling campaigns.

The work was by funded by the European Union - NextGenerationEU CRYO-RI project (grant no. 352758) and LumiMuutos project by Maa- ja vesitekniikan tuki ry. Ala-aho was supported by the Research Council of Finland SNOMLT project (grant no. 347348). Work was supported by Digital Waters (DIWA) flagship and received funding from HYDRO-RI-Platform project and the European Union – NextGenerationEU instrument funded by the Research Council of Finland under grant number 346163. Korpelainen, Kumpula and Kuzmin was supported by Research Council of Finland funded project C-NEUT (grant no. 347862).

AI tools were used to assist in code writing and text editing.

Code and data availability

The R script to run ClustSnow is available at https://github.com/jgenvironment/ClustSnow#. The data used in this study with its documentation are available at https://doi.org/10.23729/fd-561771be-24b6-354b-bdd7-1b2bb6068308 (Ylönen et al., 2025) under Creative Commons Attribution 4.0 International (CC BY 4.0) license.

Supplementary material

The supplement related to this article is available online at https://doi.org/10.23729/fd-561771be-24b6-354b-bdd7-1b2bb6068308.

860 References

- Aakala, T., Hari, P., Dengel, S., Newberry, S. L., Mizunuma, T., & Grace, J. (2014). A prominent stepwise advance of the tree line in north-east Finland. *Journal of Ecology*, 102(6), 1582–1591. https://doi.org/https://doi.org/10.1111/1365-2745.12308
- Adams, M. S., Bühler, Y., & Fromm, R. (2018). Multitemporal Accuracy and Precision Assessment of Unmanned

 Aerial System Photogrammetry for Slope-Scale Snow Depth Maps in Alpine Terrain. *Pure and Applied Geophysics*, 175(9), 3303–3324. https://doi.org/10.1007/s00024-017-1748-y
 - Ahmed, M., Seraj, R., & Islam, S. M. S. (2020). The k-means Algorithm: A Comprehensive Survey and Performance Evaluation. *Electronics*, 9(8), 1295. https://doi.org/10.3390/electronics9081295
- Ala-Aho, P., Autio, A., Bhattacharjee, J., Isokangas, E., Kujala, K., Marttila, H., Menberu, M., Meriö, L.-J., Postila, H., Rauhala, A., Ronkanen, A.-K., Rossi, P. M., Saari, M., Haghighi, A. T., & Kløve, B. (2021). What conditions favor the influence of seasonally frozen ground on hydrological partitioning? A systematic review. Environmental Research Letters, 16(4), 043008. https://doi.org/10.1088/1748-9326/abe82c

- Bavay, M., Grünewald, T., & Lehning, M. (2013). Response of snow cover and runoff to climate change in high Alpine catchments of Eastern Switzerland. *Advances in Water Resources*, 55, 4–16. https://doi.org/10.1016/J.ADVWATRES.2012.12.009
- Beaudoin-Galaise, M., & Jutras, S. (2022). Comparison of manual snow water equivalent (SWE) measurements: seeking the reference for a true SWE value in a boreal biome. *The Cryosphere*, *16*(8), 3199–3214. https://doi.org/10.5194/tc-16-3199-2022
- Berghuijs, W. R., & Hale, K. (2025). Streamflow shifts with declining snowfall. *Nature*, *638*(8052), E35–E37. https://doi.org/10.1038/s41586-024-08523-5

885

895

- Bhardwaj, A., Sam, L., Bhardwaj, A., & Martín-Torres, F. J. (2016). LiDAR remote sensing of the cryosphere: Present applications and future prospects. *Remote Sensing of Environment*, 177, 125–143. https://doi.org/10.1016/J.RSE.2016.02.031
- Bouchard, B., Nadeau, D. F., & Domine, F. (2022). Comparison of snowpack structure in gaps and under the canopy in a humid boreal forest. *Hydrological Processes*, *36*(9). https://doi.org/10.1002/hyp.14681
 - Breiman, L. (2001). Random Forests. Machine Learning, 45(1), 5-32. https://doi.org/10.1023/A:1010933404324
- Broxton, P. D., & van Leeuwen, W. J. D. (2020). Structure from Motion of Multi-Angle RPAS Imagery Complements Larger-Scale Airborne Lidar Data for Cost-Effective Snow Monitoring in Mountain Forests. *Remote Sensing*, 12(14), 2311. https://doi.org/10.3390/rs12142311
- Broxton, P. D., van Leeuwen, W. J. D., & Biederman, J. A. (2019). Improving Snow Water Equivalent Maps With Machine Learning of Snow Survey and Lidar Measurements. *Water Resources Research*, 55(5), 3739–3757. https://doi.org/10.1029/2018WR024146
 - Busseau, B. C., Royer, A., Roy, A., Langlois, A., & Domine, F. (2017). Analysis of snow-vegetation interactions in the low Arctic-Subarctic transition zone (northeastern Canada). *Physical Geography*, 38(2), 159–175. https://doi.org/10.1080/02723646.2017.1283477
 - Callaghan, T. V, Johansson, M., Brown, R. D., Groisman, P. Ya., Labba, N., Radionov, V., Bradley, R. S., Blangy, S., Bulygina, O. N., Christensen, T. R., Colman, J. E., Essery, R. L. H., Forbes, B. C., Forchhammer, M. C., Golubev, V. N., Honrath, R. E., Juday, G. P., Meshcherskaya, A. V, Phoenix, G. K., ... Wood, E. F. (2011). Multiple Effects of Changes in Arctic Snow Cover. AMBIO, 40(1), 32–45. https://doi.org/10.1007/s13280-011-0213-x
 - Charrad, M., Ghazzali, N., Boiteau, V., & Niknafs, A. (2014). Nbclust: An R package for determining the relevant number of clusters in a data set. *Journal of Statistical Software*, 61(6), 1–36. https://doi.org/10.18637/jss.v061.i06
- Colombo, N., Valt, M., Romano, E., Salerno, F., Godone, D., Cianfarra, P., Freppaz, M., Maugeri, M., & Guyennon, N. (2022). Long-term trend of snow water equivalent in the Italian Alps. *Journal of Hydrology*, *614*, 128532. https://doi.org/10.1016/j.jhydrol.2022.128532
 - Croghan, D., Ala-Aho, P., Lohila, A., Welker, J., Vuorenmaa, J., Kløve, B., Mustonen, K., Aurela, M., & Marttila, H. (2023). Coupling of Water-Carbon Interactions During Snowmelt in an Arctic Finland Catchment. Water Resources Research, 59(5). https://doi.org/10.1029/2022WR032892

Ourrier, W. R., & Lundquist, J. D. (2018). Snow Depth Variability at the Forest Edge in Multiple Climates in the Western United States. *Water Resources Research*, 54(11), 8756–8773. https://doi.org/10.1029/2018WR022553

915

925

- Currier, W. R., Sun, N., Wigmosta, M., Cristea, N., & Lundquist, J. D. (2022). The impact of forest-controlled snow variability on late-season streamflow varies by climatic region and forest structure. *Hydrological Processes*, 36(6). https://doi.org/10.1002/hyp.14614
- Deems, J. S., Painter, T. H., & Finnegan, D. C. (2013). Lidar measurement of snow depth: a review. *Journal of Glaciology*, 59(215), 467–479. https://doi.org/10.3189/2013JoG12J154
- Dharmadasa, V., Kinnard, C., & Baraër, M. (2022). An Accuracy Assessment of Snow Depth Measurements in Agro-Forested Environments by UAV Lidar. *Remote Sensing*, 14(7), 1649. https://doi.org/10.3390/rs14071649
- Dharmadasa, V., Kinnard, C., & Baraër, M. (2023). Topographic and vegetation controls of the spatial distribution of snow depth in agro-forested environments by UAV lidar. *The Cryosphere*, 17(3), 1225–1246. https://doi.org/10.5194/tc-17-1225-2023
 - Engelhardt, M., Schuler, T. V, & Andreassen, L. M. (2014). Contribution of snow and glacier melt to discharge for highly glacierised catchments in Norway. *Hydrology and Earth System Sciences*, 18(2), 511–523. https://doi.org/10.5194/hess-18-511-2014
 - Evans, J. S., & Hudak, A. T. (2007). A Multiscale Curvature Algorithm for Classifying Discrete Return LiDAR in Forested Environments. *IEEE Transactions on Geoscience and Remote Sensing*, 45(4), 1029–1038. https://doi.org/10.1109/TGRS.2006.890412
- Faquseh, H., & Grossi, G. (2024). Trend analysis of precipitation, temperature and snow water equivalent in Lombardy region, northern Italy. *Sustainable Water Resources Management*, 10(1), 18. https://doi.org/10.1007/s40899-023-00992-2
 - Fernandez-Diaz, J. C., Glennie, C. L., Carter, W. E., Shrestha, R. L., Sartori, M. P., Singhania, A., Legleiter, C. J., & Overstreet, B. T. (2014). Early Results of Simultaneous Terrain and Shallow Water Bathymetry Mapping Using a Single-Wavelength Airborne LiDAR Sensor. *IEEE Journal of Selected Topics in Applied Earth Observations and Remote Sensing*, 7(2), 623–635. https://doi.org/10.1109/JSTARS.2013.2265255
 - Fontrodona-Bach, A., Schaefli, B., Woods, R., Teuling, A. J., & Larsen, J. R. (2023). NH-SWE: Northern Hemisphere Snow Water Equivalent dataset based on in situ snow depth time series. *Earth System Science Data*, 15(6), 2577–2599. https://doi.org/10.5194/essd-15-2577-2023
- Franke, A. K., Bräuning, A., Timonen, M., & Rautio, P. (2017). Growth response of Scots pines in polar-alpine treeline to a warming climate. *Forest Ecology and Management*, 399, 94–107. https://doi.org/10.1016/J.FORECO.2017.05.027
 - Fujihara, Y., Takase, K., Chono, S., Ichion, E., Ogura, A., & Tanaka, K. (2017). Influence of topography and forest characteristics on snow distributions in a forested catchment. *Journal of Hydrology*, *546*, 289–298. https://doi.org/10.1016/j.jhydrol.2017.01.021
- Gaffey, C., & Bhardwaj, A. (2020). Applications of Unmanned Aerial Vehicles in Cryosphere: Latest Advances and Prospects. *Remote Sensing*, *12*(6), 948. https://doi.org/10.3390/rs12060948

- Geissler, J., Mazzotti, G., Rathmann, L., Webster, C., & Weiler, M. (2024). ClustSnow: Utilizing temporally persistent forest snow patterns under variable environmental conditions. https://doi.org/10.22541/essoar.172222597.78203131/v1
- Geissler, J., Rathmann, L., & Weiler, M. (2023). Combining Daily Sensor Observations and Spatial LiDAR Data for Mapping Snow Water Equivalent in a Sub-Alpine Forest. Water Resources Research, 59(9), e2023WR034460. https://doi.org/https://doi.org/10.1029/2023WR034460
 - Gottlieb, A. R., & Mankin, J. S. (2024). Evidence of human influence on Northern Hemisphere snow loss. *Nature*, 625(7994), 293–300. https://doi.org/10.1038/s41586-023-06794-y
- Grace, J., Berningen, F., & Nagy, L. (2002). Impacts of Climate Change on the Tree Line. *Annals of Botany*, 90(4), 537–544. https://doi.org/10.1093/aob/mcf222
 - Harder, P., Pomeroy, J. W., & Helgason, W. D. (2020). Improving sub-canopy snow depth mapping with unmanned aerial vehicles: lidar versus structure-from-motion techniques. *The Cryosphere*, *14*(6), 1919–1935. https://doi.org/10.5194/tc-14-1919-2020
- Hartigan, J. A., & Wong, M. A. (1979). Algorithm AS 136: A K-Means Clustering Algorithm. Applied Statistics, 28(1), 100. https://doi.org/10.2307/2346830
 - Jacobs, J. M., Hunsaker, A. G., Sullivan, F. B., Palace, M., Burakowski, E. A., Herrick, C., & Cho, E. (2021). Snow depth mapping with unpiloted aerial system lidar observations: a case study in Durham, New Hampshire, United States. *The Cryosphere*, 15(3), 1485–1500. https://doi.org/10.5194/tc-15-1485-2021
- Jan, A., & Painter, S. L. (2020). Permafrost thermal conditions are sensitive to shifts in snow timing. *Environmental Research Letters*, 15(8), 84026. https://doi.org/10.1088/1748-9326/ab8ec4
 - King, F., Erler, A. R., Frey, S. K., & Fletcher, C. G. (2020). Application of machine learning techniques for regional bias correction of snow water equivalent estimates in Ontario, Canada. *Hydrology and Earth System Sciences*, 24(10), 4887–4902. https://doi.org/10.5194/hess-24-4887-2020
- 6970 Koutantou, K., Mazzotti, G., Brunner, P., Webster, C., & Jonas, T. (2022). Exploring snow distribution dynamics in steep forested slopes with UAV-borne LiDAR. *Cold Regions Science and Technology*, 200, 103587. https://doi.org/10.1016/j.coldregions.2022.103587

- Kunkel, K. E., Robinson, D. A., Champion, S., Yin, X., Estilow, T., & Frankson, R. M. (2016). Trends and Extremes in Northern Hemisphere Snow Characteristics. *Current Climate Change Reports*, 2(2), 65–73. https://doi.org/10.1007/s40641-016-0036-8
- Kuusisto, E. (1984). Snow accumulation and snowmelt in Finland. In *Publications of the water research institute* (55th ed.). National Board of Waters.
- Langlois, A., Kohn, J., Royer, A., Cliche, P., Brucker, L., Picard, G., Fily, M., Derksen, C., & Willemet, J. M. (2009).
 Simulation of Snow Water Equivalent (SWE) Using Thermodynamic Snow Models in Québec, Canada. *Journal of Hydrometeorology*, 10(6), 1447–1463. https://doi.org/10.1175/2009JHM1154.1
- Li, Q., Ma, M., Wu, X., & Yang, H. (2018). Snow Cover and Vegetation-Induced Decrease in Global Albedo From 2002 to 2016. *Journal of Geophysical Research: Atmospheres*, 123(1), 124–138. https://doi.org/10.1002/2017JD027010

- Lundquist, J. D., Dickerson-Lange, S. E., Lutz, J. A., & Cristea, N. C. (2013). Lower forest density enhances snow retention in regions with warmer winters: A global framework developed from plot-scale observations and modeling. *Water Resources Research*, 49(10), 6356–6370. https://doi.org/10.1002/wrcr.20504
 - Luomaranta, A., Aalto, J., & Jylhä, K. (2019). Snow cover trends in Finland over 1961–2014 based on gridded snow depth observations. *International Journal of Climatology*, 39(7), 3147–3159. https://doi.org/https://doi.org/10.1002/joc.6007
- Maier, K., Nascetti, A., van Pelt, W., & Rosqvist, G. (2022). Direct photogrammetry with multispectral imagery for UAV-based snow depth estimation. ISPRS Journal of Photogrammetry and Remote Sensing, 186, 1–18. https://doi.org/10.1016/J.ISPRSJPRS.2022.01.020

1000

- Malek, S. A., Bales, R. C., & Glaser, S. D. (2020). Estimation of Daily Spatial Snow Water Equivalent from Historical Snow Maps and Limited In-Situ Measurements. *Hydrology*, 7(3), 46. https://doi.org/10.3390/hydrology7030046
- Marttila, H., Lohila, A., Ala-Aho, P., Noor, K., Welker, J. M., Croghan, D., Mustonen, K., Meriö, L., Autio, A., Muhic, F., Bailey, H., Aurela, M., Vuorenmaa, J., Penttilä, T., Hyöky, V., Klein, E., Kuzmin, A., Korpelainen, P., Kumpula, T., ... Kløve, B. (2021). Subarctic catchment water storage and carbon cycling Leading the way for future studies using integrated datasets at Pallas, Finland. *Hydrological Processes*, 35(9). https://doi.org/10.1002/hyp.14350
- Matiu, M., Crespi, A., Bertoldi, G., Carmagnola, C. M., Marty, C., Morin, S., Schöner, W., Cat Berro, D., Chiogna, G., De Gregorio, L., Kotlarski, S., Majone, B., Resch, G., Terzago, S., Valt, M., Beozzo, W., Cianfarra, P., Gouttevin, I., Marcolini, G., ... Weilguni, V. (2021). Observed snow depth trends in the European Alps: 1971 to 2019. *The Cryosphere*, 15(3), 1343–1382. https://doi.org/10.5194/tc-15-1343-2021
- Matti, B., Dahlke, H., Dieppois, B., Lawler, D., & Lyon, S. (2017). Flood seasonality across Scandinavia Evidence of a shifting hydrograph? *Hydrological Processes*, *31*. https://doi.org/10.1002/hyp.11365
 - Mazzotti, G., Currier, W. R., Deems, J. S., Pflug, J. M., Lundquist, J. D., & Jonas, T. (2019). Revisiting Snow Cover Variability and Canopy Structure Within Forest Stands: Insights From Airborne Lidar Data. Water Resources Research, 55(7), 6198–6216. https://doi.org/https://doi.org/10.1029/2019WR024898
- Mazzotti, G., Essery, R., Moeser, C. D., & Jonas, T. (2020). Resolving Small-Scale Forest Snow Patterns Using an Energy Balance Snow Model With a One-Layer Canopy. *Water Resources Research*, 56(1). https://doi.org/10.1029/2019WR026129
 - Mazzotti, G., Webster, C., Essery, R., & Jonas, T. (2021). Increasing the Physical Representation of Forest-Snow Processes in Coarse-Resolution Models: Lessons Learned From Upscaling Hyper-Resolution Simulations. *Water Resources Research*, 57(5), e2020WR029064. https://doi.org/https://doi.org/10.1029/2020WR029064
 - Mazzotti, G., Webster, C., Quéno, L., Cluzet, B., & Jonas, T. (2023). Canopy structure, topography, and weather are equally important drivers of small-scale snow cover dynamics in sub-alpine forests. *Hydrology and Earth System Sciences*, 27(11), 2099–2121. https://doi.org/10.5194/hess-27-2099-2023

Meriö, L., Ala-aho, P., Linjama, J., Hjort, J., Kløve, B., & Marttila, H. (2019). Snow to Precipitation Ratio Controls

Catchment Storage and Summer Flows in Boreal Headwater Catchments. *Water Resources Research*, 55(5),

4096–4109. https://doi.org/10.1029/2018WR023031

1025

1030

- Meriö, L.-J., Rauhala, A., Ala-aho, P., Kuzmin, A., Korpelainen, P., Kumpula, T., Kløve, B., & Marttila, H. (2023). Measuring the spatiotemporal variability in snow depth in subarctic environments using UASs Part 2: Snow processes and snow–canopy interactions. *The Cryosphere*, 17(10), 4363–4380. https://doi.org/10.5194/tc-17-4363-2023
- Mooney, P. A., & Li, L. (2021). Near future changes to rain-on-snow events in Norway. *Environmental Research Letters*, 16(6), 064039. https://doi.org/10.1088/1748-9326/abfdeb
- Morissette, L., & Chartier, S. (2013). The k-means clustering technique: General considerations and implementation in Mathematica. *Tutorials in Quantitative Methods for Psychology*, 9(1), 15–24. https://doi.org/10.20982/tqmp.09.1.p015
- Mortimer, C., Mudryk, L., Derksen, C., Luojus, K., Brown, R., Kelly, R., & Tedesco, M. (2020). Evaluation of long-term Northern Hemisphere snow water equivalent products. *The Cryosphere*, 14(5), 1579–1594. https://doi.org/10.5194/tc-14-1579-2020
- Mudryk, L. R., Kushner, P. J., Derksen, C., & Thackeray, C. (2017). Snow cover response to temperature in observational and climate model ensembles. *Geophysical Research Letters*, 44(2), 919–926. https://doi.org/https://doi.org/10.1002/2016GL071789
 - Mudryk, L., Santolaria-Ot\'{\i}n, M., Krinner, G., Ménégoz, M., Derksen, C., Brutel-Vuilmet, C., Brady, M., & Essery, R. (2020). Historical Northern Hemisphere snow cover trends and projected changes in the CMIP6 multi-model ensemble. *The Cryosphere*, 14(7), 2495–2514. https://doi.org/10.5194/tc-14-2495-2020
- Muhic, F., Ala-Aho, P., Noor, K., Welker, J. M., Klöve, B., & Marttila, H. (2023). Flushing or mixing? Stable water isotopes reveal differences in arctic forest and peatland soil water seasonality. *Hydrological Processes*, *37*(1). https://doi.org/10.1002/hyp.14811
 - Muhuri, A., Gascoin, S., Menzel, L., Kostadinov, T. S., Harpold, A. A., Sanmiguel-Vallelado, A., & Lopez-Moreno, J. I. (2021). Performance Assessment of Optical Satellite-Based Operational Snow Cover Monitoring Algorithms in Forested Landscapes. *IEEE Journal of Selected Topics in Applied Earth Observations and Remote Sensing*, 14, 7159–7178. https://doi.org/10.1109/JSTARS.2021.3089655
 - Mustonen, S. (1965). Ilmasto- ja maastotekijöiden vaikutuksesta lumen vesiarvoon ja roudan syvyyteen. *Acta Forestalia Fennica*, 79(1). https://doi.org/10.14214/aff.7159
- Niedzielski, T., Spallek, W., & Witek-Kasprzak, M. (2018). Automated Snow Extent Mapping Based on Orthophoto

 Images from Unmanned Aerial Vehicles. *Pure and Applied Geophysics*, 175(9), 3285–3302. https://doi.org/10.1007/s00024-018-1843-8
 - Nolan, M., Larsen, C., & Sturm, M. (2015). Mapping snow depth from manned aircraft on landscape scales at centimeter resolution using structure-from-motion photogrammetry. *The Cryosphere*, 9(4), 1445–1463. https://doi.org/10.5194/tc-9-1445-2015

- Okkonen, J., Ala-Aho, P., Hänninen, P., Hayashi, M., Sutinen, R., & Liwata, P. (2017). Multi-year simulation and model calibration of soil moisture and temperature profiles in till soil. *European Journal of Soil Science*, 68(6), 829–839. https://doi.org/https://doi.org/10.1111/ejss.12489
 - Painter, T. H., Berisford, D. F., Boardman, J. W., Bormann, K. J., Deems, J. S., Gehrke, F., Hedrick, A., Joyce, M., Laidlaw, R., Marks, D., Mattmann, C., McGurk, B., Ramirez, P., Richardson, M., Skiles, S. M., Seidel, F. C., & Winstral, A. (2016). The Airborne Snow Observatory: Fusion of scanning lidar, imaging spectrometer, and physically-based modeling for mapping snow water equivalent and snow albedo. *Remote Sensing of Environment*, 184, 139–152. https://doi.org/10.1016/j.rse.2016.06.018

1075

- Pall, P., Tallaksen, L. M., & Stordal, F. (2019). A Climatology of Rain-on-Snow Events for Norway. *Journal of Climate*, 32(20), 6995–7016. https://doi.org/10.1175/JCLI-D-18-0529.1
- Paul, J. D., Buytaert, W., & Sah, N. (2020). A Technical Evaluation of Lidar-Based Measurement of River Water Levels. *Water Resources Research*, 56(4). https://doi.org/10.1029/2019WR026810
 - Pflug, J. M., & Lundquist, J. D. (2020). Inferring Distributed Snow Depth by Leveraging Snow Pattern Repeatability: Investigation Using 47 Lidar Observations in the Tuolumne Watershed, Sierra Nevada, California. *Water Resources Research*, 56(9), e2020WR027243. https://doi.org/https://doi.org/10.1029/2020WR027243
- Pilarska, M., Ostrowski, W., Bakuła, K., Górski, K., & Kurczyński, Z. (2016). The potential of light laser scanners developed for unmanned aerial vehicles the review and accuracy. *The International Archives of the Photogrammetry, Remote Sensing and Spatial Information Sciences*, XLII-2/W2, 87–95. https://doi.org/10.5194/isprs-archives-XLII-2-W2-87-2016
 - R Core Team. (2023). R: A language and environment for statistical computing. . R Foundation for Statistical Computing. https://www.R-project.org/
 - Räisänen, J. (2023). Changes in March mean snow water equivalent since the mid-20th century and the contributing factors in reanalyses and CMIP6 climate models. *The Cryosphere*, 17(5), 1913–1934. https://doi.org/10.5194/tc-17-1913-2023
- Rauhala, A., Meriö, L.-J., Kuzmin, A., Korpelainen, P., Ala-aho, P., Kumpula, T., Kløve, B., & Marttila, H. (2023).

 Measuring the spatiotemporal variability in snow depth in subarctic environments using UASs Part 1:

 Measurements, processing, and accuracy assessment. *The Cryosphere*, 17(10), 4343–4362.

 https://doi.org/10.5194/tc-17-4343-2023
 - Revuelto, J., Alonso-González, E., & López-Moreno, J. I. (2020). Generation of daily high-spatial resolution snow depth maps from in-situ measurement and time-lapse photographs. *Cuadernos de Investigación Geográfica*, 46(1), 59–79. https://doi.org/10.18172/cig.3801
 - Revuelto, J., López-Moreno, J. I., & Alonso-González, E. (2021). Light and Shadow in Mapping Alpine Snowpack With Unmanned Aerial Vehicles in the Absence of Ground Control Points. *Water Resources Research*, *57*(6). https://doi.org/10.1029/2020WR028980
- Rittger, K., Raleigh, M. S., Dozier, J., Hill, A. F., Lutz, J. A., & Painter, T. H. (2020). Canopy Adjustment and Improved Cloud Detection for Remotely Sensed Snow Cover Mapping. *Water Resources Research*, *56*(6). https://doi.org/10.1029/2019WR024914

- Rogers, S. R., Manning, I., & Livingstone, W. (2020). Comparing the Spatial Accuracy of Digital Surface Models from Four Unoccupied Aerial Systems: Photogrammetry Versus LiDAR. *Remote Sensing*, *12*(17), 2806. https://doi.org/10.3390/rs12172806
- Ropars, P., & Boudreau, S. (2012). Shrub expansion at the forest–tundra ecotone: spatial heterogeneity linked to local topography. *Environmental Research Letters*, 7(1), 015501. https://doi.org/10.1088/1748-9326/7/1/015501

1105

1110

- Ruosteenoja, K., Markkanen, T., & Räisänen, J. (2020). Thermal seasons in northern Europe in projected future climate. *International Journal of Climatology*, 40(10), 4444–4462. https://doi.org/10.1002/joc.6466
- Stillinger, T., Rittger, K., Raleigh, M. S., Michell, A., Davis, R. E., & Bair, E. H. (2023). Landsat, MODIS, and VIIRS snow cover mapping algorithm performance as validated by airborne lidar datasets. *The Cryosphere*, 17(2), 567–590. https://doi.org/10.5194/tc-17-567-2023
- Stuefer, S. L., Kane, D. L., & Dean, K. M. (2020). Snow Water Equivalent Measurements in Remote Arctic Alaska Watersheds. *Water Resources Research*, 56(4). https://doi.org/10.1029/2019WR025621
- Sturm, M., & Wagner, A. M. (2010). Using repeated patterns in snow distribution modeling: An Arctic example. *Water Resources Research*, 46(12). https://doi.org/10.1029/2010WR009434
- The Finnish meteorological institute. (2025). *Säähavaintojen vuorokausi- ja kuukausiarvot*. Https://Www.Ilmatieteenlaitos.Fi/Avoin-Data-Saahavaintojen-Vrk-Ja-Kk-Arvot.
- Thiebault, K., & Young, S. (2020). Snow cover change and its relationship with land surface temperature and vegetation in northeastern North America from 2000 to 2017. *International Journal of Remote Sensing*, 41(21), 8453–8474. https://doi.org/10.1080/01431161.2020.1779379
- Trujillo, E., Ramírez, J. A., & Elder, K. J. (2007). Topographic, meteorologic, and canopy controls on the scaling characteristics of the spatial distribution of snow depth fields. *Water Resources Research*, 43(7). https://doi.org/10.1029/2006WR005317
- Tsang, L., Durand, M., Derksen, C., Barros, A. P., Kang, D.-H., Lievens, H., Marshall, H.-P., Zhu, J., Johnson, J.,
 King, J., Lemmetyinen, J., Sandells, M., Rutter, N., Siqueira, P., Nolin, A., Osmanoglu, B., Vuyovich, C., Kim,
 E., Taylor, D., ... Xu, X. (2022a). Review article: Global monitoring of snow water equivalent using high-frequency radar remote sensing. *The Cryosphere*, 16(9), 3531–3573. https://doi.org/10.5194/tc-16-3531-2022
 - Tsang, L., Durand, M., Derksen, C., Barros, A. P., Kang, D.-H., Lievens, H., Marshall, H.-P., Zhu, J., Johnson, J., King, J., Lemmetyinen, J., Sandells, M., Rutter, N., Siqueira, P., Nolin, A., Osmanoglu, B., Vuyovich, C., Kim, E., Taylor, D., ... Xu, X. (2022b). Review article: Global monitoring of snow water equivalent using high-frequency radar remote sensing. *The Cryosphere*, *16*(9), 3531–3573. https://doi.org/10.5194/tc-16-3531-2022
 - Vafakhah, M., Nasiri Khiavi, A., Janizadeh, S., & Ganjkhanlo, H. (2022). Evaluating different machine learning algorithms for snow water equivalent prediction. *Earth Science Informatics*, 15(4), 2431–2445. https://doi.org/10.1007/s12145-022-00846-z
- Vionnet, V., Brun, E., Morin, S., Boone, A., Faroux, S., Le Moigne, P., Martin, E., & Willemet, J.-M. (2012). The detailed snowpack scheme Crocus and its implementation in SURFEX v7.2. *Geoscientific Model Development*, 5(3), 773–791. https://doi.org/10.5194/gmd-5-773-2012

- Wang, R., Kumar, M., & Link, T. E. (2016). Potential trends in snowmelt-generated peak streamflows in a warming climate. *Geophysical Research Letters*, 43(10), 5052–5059. https://doi.org/https://doi.org/10.1002/2016GL068935
- Winkler, M., Schellander, H., & Gruber, S. (2021). Snow water equivalents exclusively from snow depths and their temporal changes: the Δsnow model. *Hydrology and Earth System Sciences*, 25(3), 1165–1187. https://doi.org/10.5194/hess-25-1165-2021
- Woods, S. W., Ahl, R., Sappington, J., & McCaughey, W. (2006). Snow accumulation in thinned lodgepole pine stands, Montana, USA. *Forest Ecology and Management*, 235(1–3), 202–211. https://doi.org/10.1016/j.foreco.2006.08.013

- Yang, Z., Chen, R., Liu, Y., Zhao, Y., Liu, Z., & Liu, J. (2023). The impact of rain-on-snow events on the snowmelt process: A field study. *Hydrological Processes*, *37*(11). https://doi.org/10.1002/hyp.15019
- Zhang, J., Pohjola, V. A., Pettersson, R., Norell, B., Marchand, W.-D., Clemenzi, I., & Gustafsson, D. (2021).

 Improving the snowpack monitoring in the mountainous areas of Sweden from space: a machine learning approach. *Environmental Research Letters*, 16(8), 84007. https://doi.org/10.1088/1748-9326/abfe8d
 - Zhang, Y., & Ma, N. (2018). Spatiotemporal variability of snow cover and snow water equivalent in the last three decades over Eurasia. *Journal of Hydrology*, 559, 238–251. https://doi.org/10.1016/j.jhydrol.2018.02.031